

Study of MSSM heavy Higgs bosons decaying into charginos and neutralinos

Rahool K. Barman,^a Biplob Bhattacharjee,^a Amit Chakraborty,^b and Arghya Choudhury^{c,d}

^a*Centre for High Energy Physics,*

Indian Institute of Science, Bangalore 560012, India

^b*Department of Theoretical Physics, Tata Institute of Fundamental Research,*

1, Homi Bhabha Road, Mumbai 400005, India

^c*Consortium for Fundamental Physics, Department of Physics and Astronomy,*

University of Sheffield, Sheffield S3 7RH, United Kingdom

^d*Consortium for Fundamental Physics, Department of Physics and Astronomy,*

University of Manchester, Manchester, M13 9PL, United Kingdom

*E-mail: rahoolkbarman@chep.iisc.ernet.in, biplob@chep.iisc.ernet.in,
amit@theory.tifr.res.in, a.choudhury@sheffield.ac.uk*

ABSTRACT: A multitude of searches have already been performed by the ATLAS and CMS collaborations at the LHC to probe the heavy Higgses of the Minimal Supersymmetric Standard Model (MSSM) through their decay to the Standard Model particles. In this paper, we study the decay of the MSSM heavy Higgses into neutralino and chargino pairs and estimate the maximum possible branching ratios for these ‘ino’ modes being consistent with the present LHC data. After performing a random scan of the relevant electroweakino parameters, we impose the SM 125 GeV Higgs constraints, low energy flavour data as well as current bounds on heavy Higgses from the LHC run-I and run-II data. The present limits on the electroweakino masses and couplings are also considered in our analysis. We choose a few representative benchmark points satisfying all the above-mentioned constraints, and then perform a detailed collider simulation, including fast detector effects, and analyze all the potential SM backgrounds in order to estimate the discovery reach of these heavy Higgses at the LHC. We restrict ourselves within the leptonic cascade decay modes of these heavy Higgses and study the mono- $X + \cancel{E}_T$ ($X=W,Z$) and trilepton + \cancel{E}_T signatures in the context of high luminosity run of the 14 TeV LHC.

Contents

1	Introduction	2
2	Available parameter space and LHC data	4
2.1	Higgs couplings to Electroweakinos	4
2.2	Experimental inputs and Parameter space scan	8
2.3	SUSY decay of Heavy Higgses and the allowed parameter space	10
2.4	Current LHC bounds for heavy Higgs sector and electroweakinos	16
2.4.1	Search for H with $\gamma\gamma$ final states	16
2.4.2	Search for H with WW final states	16
2.4.3	Search for H with ZZ final states	17
2.4.4	Search for H with hh final states	17
2.4.5	Search for H/A with $\tau^+\tau^-$ final states	17
2.4.6	Search for A with Zh final states	18
2.4.7	Search for H^\pm with $\tau\nu$ and $t\bar{b}$ final states	18
2.4.8	Current LHC bounds for electroweakinos	19
3	Search strategies and Future limits	20
3.1	Benchmark points	20
3.2	Mono-X plus missing energy	24
3.2.1	Mono-Z (leptonic) + \cancel{E}_T channel	24
3.2.2	Mono-W (leptonic) + \cancel{E}_T channel	26
3.3	Trilepton + \cancel{E}_T channel	27
4	Summary	29

1 Introduction

The observation of a resonance around 125 GeV by the ATLAS and CMS collaborations has led to a new era in particle physics [1, 2]. Comprehensive studies to investigate the spin and parity quantum numbers of the observed particle prefer its scalar nature. Various properties of this newly discovered resonance also seem to be in good accordance with that of the Standard Model (SM) Higgs boson. However, it is to be noted that even though large deviations from the SM predictions have already been excluded from the current LHC data, non-standard Higgs couplings are still allowed within the present uncertainties in various Higgs coupling measurements [3–5]. Thus, the possibility of the observed resonance being a part of an extended Higgs sector is not ruled out by the current LHC data, what we require is very precise measurement of various couplings of the observed Higgs boson to the SM particles.

Supersymmetry (SUSY) [6–8] has been so far one of the most popular framework for formulating physics beyond the SM (BSM), however a SUSY signature is yet to be observed at the LHC [9, 10]. The Higgs sector of the Minimal Supersymmetric Standard Model (MSSM) is phenomenologically richer compared to that of the SM [7, 8]. The model has two CP-even neutral Higgses (the lighter and the heavier ones are h and H respectively), one CP-odd neutral Higgs (A) and two charged scalars (H^\pm). At the tree level, the Higgs sector of the MSSM can be parametrised by two parameters - $\tan\beta$, the ratio of the vev of the two Higgs doublets ($H_{u,d}$), and the pseudoscalar Higgs mass M_A . In MSSM, the lightest CP even Higgs boson has a mass which lies below M_Z at the tree level. To reconcile the observed Higgs mass at 125 GeV, one needs to invoke large higher order loop corrections involving the SM and SUSY particles. Soon after the Higgs discovery, numerous studies have been performed to look for additional Higgs-like states by both the ATLAS and CMS collaborations at the LHC. For example, both the ATLAS and CMS collaborations have studied the decay of the CP-even heavy scalar boson (H) into a pair of photons [11, 12], W bosons [13, 14], Z bosons [15] and SM-like 125 GeV Higgs bosons (h) [16–20] through various possible final state topologies. The decay of the CP-odd pseudoscalar Higgs boson (A) into a h and Z boson has also been studied at $\sqrt{s} = 8$ TeV data by both the LHC collaborations [21, 22]. Moreover, the decay of the neutral Higgs bosons H/A to a pair of tau-leptons has also been studied by the ATLAS and CMS collaboration using $\sqrt{s} = 7$ TeV and $\sqrt{s} = 8$ TeV data [23, 24]. This search mode has been found to be by far one of the most efficient channels to constrain the MSSM parameter space. For example, using $H/A \rightarrow \tau^+\tau^-$ channel, regions with large $\tan\beta$ (say > 20) and small M_A (say < 500 GeV) are already excluded by LHC run-II data. Comprehensive studies have also been performed to search for the charged Higgs bosons. The CMS collaboration has looked for the charged Higgses via its decay to $\tau^+\nu_\tau$ and $t\bar{b}$, when H^\pm is produced from the $t\bar{t}$ and/or $pp \rightarrow \bar{t}(b)H^\pm$ processes [25, 26]. Studies of H^\pm decaying to a tau lepton and a neutrino has been performed by the ATLAS collaboration using dataset collected at $\sqrt{s} = 8$ TeV corresponding to an integrated luminosity of 19.5 fb^{-1} [27, 28]. All the above mentioned studies have not been able to find any compelling signature of the heavy Higgs bosons, and hence 95% C.L. upper limits on the production cross-section times the branching ratios have been placed for a wide range of MSSM heavy resonance masses.

From the above discussions it is clear that all of the aforementioned LHC analyses of the MSSM

neutral and charged Higgs bosons rely on their decay to the SM particles. However, we have to keep in mind that the decay of these heavy MSSM Higgses to light supersymmetric particles, if kinematically allowed, would modify the branching ratios of the heavy Higgses to SM particles considerably. Let's consider an example: a CP even heavy Higgs H can decay, if kinematically allowed, to a pair of neutralinos which then decays to SM Higgs and/or Z and the lightest neutralino with h/Z decaying through their usual decay modes. A few sample processes are shown below,

$$\begin{aligned} H, A &\rightarrow \tilde{\chi}_2^0 + \tilde{\chi}_1^0, & \tilde{\chi}_2^0 &\rightarrow h/Z + \tilde{\chi}_1^0, \\ H, A &\rightarrow \tilde{\chi}_2^0 + \tilde{\chi}_3^0, & \tilde{\chi}_2^0 &\rightarrow h/Z + \tilde{\chi}_1^0, & \tilde{\chi}_3^0 &\rightarrow h/Z + \tilde{\chi}_2^0. \end{aligned}$$

Many such processes are possible, when these decays are kinematically allowed, and most of these decays lead to a wide range of final state topologies which can be tested at the LHC. Study of this very interesting possibility is the key motivation of this paper. One can ask the following set of questions: (a) What are the relative branching ratios of the heavy Higgses decaying into the electroweakinos (i.e., charginos and neutralinos) ? (b) How large/small these heavy Higgs decay modes can be satisfying the LHC run-I & run-II Higgs data ? and, finally (c) Do the run-II and future high luminosity runs of the LHC have the sensitivity to search for these heavy resonances through these electroweakino channels ? In this paper, we attempt to answer these question by performing parameter space scan satisfying current LHC data and then analyzing the decay of the MSSM heavy Higgses to electroweakinos through mono- X plus missing energy ($X=W, Z$) and the trilepton plus missing energy signatures with a detailed collider study. Here we restrict ourselves within this mono- X and trilepton searches as these analyses are simpler and also well understood in the context of LHC. Moreover, note that the branching ratios of the neutralinos/charginos to W, Z involved final states are quite large and thus we expect to have better sensitivity through these modes. Earlier phenomenological studies on the decay of H and A to pair of charginos and neutralinos can be seen in Refs. [29–42]. One loop effects on these decay modes have also been estimated [43–45]. From the experimental front, preliminary studies by the ATLAS and CMS collaborations have shown that the regions of the parameter space with heavy Higgs masses around 200 - 500 GeV decaying to neutralinos/charginos can be probed with 100/300 fb⁻¹ of luminosity at the 14 TeV run of LHC [46, 47]. The plan of this paper can be summarized as,

- We first demand that the properties of the lightest Higgs boson (h) is consistent with that of the observed 125 GeV Higgs boson satisfying all the present constraints from the 7 & 8 TeV LHC data. We restrict ourselves within the R-parity conserving SUSY where the lightest supersymmetric particle (LSP), here the lightest neutralino $\tilde{\chi}_1^0$, is stable and constitutes a source of missing transverse energy (\cancel{E}_T).
- We then perform a random scan of the relevant MSSM parameters and then satisfy the updated 125 GeV Higgs data and low energy flavour data. After discussing salient features of the parameter space allowed by the above two constraints, we choose few representative benchmark points satisfying the current LHC bounds on the heavy Higgses as well as electroweakinos.
- Finally, we perform dedicated collider studies for the heavy Higgses associated to the selected benchmark points through mono- X ($X = W, Z$) plus missing energy as well as trilepton plus missing energy (\cancel{E}_T) signatures in the context of 14 TeV high luminosity run of the LHC.

The rest of this paper is organized in the following order: we discuss the coupling of the MSSM Higgs bosons h, H, A and H^\pm to electroweakino pairs in Sec.2.1. In Sec.2.2 and 2.3, we discuss the various constraints used in our analysis and followed by the details of the parameter space scan. Existing collider bounds on the heavy Higgses and electroweakino masses are discussed in Sec.2.4 followed by a discussion on some representative benchmark points in Sec.3.1. The collider phenomenology focusing on the mono- $X + E_T^{\text{miss}}$ ($X = W/Z$) and trilepton $+ E_T$ states arising from the decay of the heavy Higgses to electroweakinos are discussed in Sec.3.2 and Sec.3.3. Finally, we summarize our results in Sec.4.

2 Available parameter space and LHC data

2.1 Higgs couplings to Electroweakinos

The decay of the MSSM heavy Higgs bosons to electroweakinos, namely charginos and neutralinos, crucially depends on the chargino/neutralino mixing matrices. The decay width of a generic Higgs boson H_k (with $k=1,2,3,4$ representing the h, H, A and H^\pm Higgses respectively) to pair of neutralinos ($\tilde{\chi}_1^0, \tilde{\chi}_2^0, \tilde{\chi}_3^0, \tilde{\chi}_4^0$) and charginos ($\tilde{\chi}_1^\pm, \tilde{\chi}_2^\pm$) can be written as [8]:

$$\Gamma(H_k \rightarrow \tilde{\chi}_i \tilde{\chi}_j) \sim M_{H_k} \left[\left((g_{ijk}^L)^2 + (g_{ijk}^R)^2 \right) \left(1 - \frac{m_{\tilde{\chi}_i}^2}{M_{H_k}^2} - \frac{m_{\tilde{\chi}_j}^2}{M_{H_k}^2} \right) - 4\epsilon_i \epsilon_j g_{ijk}^L g_{ijk}^R \frac{m_{\tilde{\chi}_i} m_{\tilde{\chi}_j}}{M_{H_k}^2} \right], \quad (2.1)$$

where $\epsilon_i = \pm 1$ denotes the sign of the i -th eigenvalue of the neutralino mass matrix, while $\epsilon_i = 1$ the same for charginos with $\tilde{\chi}_i, \tilde{\chi}_j$ representing generic electroweakinos. The left- and right-handed couplings associated to the neutral Higgs bosons ($H_\ell = h, H, A$ respectively with $\ell = 1, 2, 3$) with the neutralinos and charginos can be written as,

$$g_{\tilde{\chi}_i^0 \tilde{\chi}_j^0 H_\ell}^L = \frac{1}{2s_w} (N_{j2} - \tan \theta_w N_{j1}) (e_\ell N_{i3} + d_\ell N_{i4}) + i \leftrightarrow j \quad (2.2)$$

$$g_{\tilde{\chi}_i^0 \tilde{\chi}_j^0 H_\ell}^R = \frac{1}{2s_w} (N_{j2} - \tan \theta_w N_{j1}) (e_\ell N_{i3} + d_\ell N_{i4}) \epsilon_\ell + i \leftrightarrow j \quad (2.3)$$

$$g_{\tilde{\chi}_i^+ \tilde{\chi}_j^- H_\ell}^L = \frac{1}{\sqrt{2}s_w} (e_\ell V_{j1} U_{i2} - d_\ell V_{j2} U_{i1}) \quad (2.4)$$

$$g_{\tilde{\chi}_i^+ \tilde{\chi}_j^- H_\ell}^R = \frac{1}{\sqrt{2}s_w} (e_\ell V_{i1} U_{j2} - d_\ell V_{i2} U_{j1}) \epsilon_\ell, \quad (2.5)$$

while the same couplings for the charged Higgs bosons are given by,

$$g_{\tilde{\chi}_i^\pm \tilde{\chi}_j^0 H^\mp}^L = \frac{\cos \beta}{s_w} \left[N_{j4} V_{i1} + \frac{1}{\sqrt{2}} (N_{j2} + \tan \theta_w N_{j1}) V_{i2} \right] \quad (2.6)$$

$$g_{\tilde{\chi}_i^\pm \tilde{\chi}_j^0 H^\mp}^R = \frac{\sin \beta}{s_w} \left[N_{j3} U_{i1} + \frac{1}{\sqrt{2}} (N_{j2} + \tan \theta_w N_{j1}) U_{i2} \right]. \quad (2.7)$$

The coefficients e_ℓ and d_ℓ have the following definitions:

$$e_1 = \cos \alpha, \quad e_2 = -\sin \alpha, \quad e_3 = \sin \beta, \quad d_1 = -\sin \alpha, \quad d_2 = \cos \alpha, \quad d_3 = \cos \beta,$$

and $\epsilon_{1,2} = 1, \epsilon_3 = -1$ with $s_w = \sin \theta_w$ (θ_w being the weinberg angle), α being the Higgs mixing angle and $\tan \beta$ the ratio of vacuum expectation value of the MSSM two Higgs doublets.

From the above-mentioned equations (2.2) - (2.7), one can observe that the couplings of the MSSM Higgses with the electroweakinos crucially depend on their compositions. It is evident that the Higgses will couple with the neutralinos and charginos if and only if there exist admixture of the higgsinos and gauginos in the electroweakino mass eigenstates. The coupling of the Higgs bosons with ‘ino’ pairs would be highly suppressed if both the inos are either higgsino dominated or gaugino dominated. Now, for example, let’s consider the limit $M_1 < M_2 \ll \mu$. From the neutralino mass matrix we observe that the lightest mass eigenstate $\tilde{\chi}_1^0$ will be bino dominated and $\tilde{\chi}_2^0$ will be wino dominated, while $\tilde{\chi}_3^0$ and $\tilde{\chi}_4^0$ are higgsino dominated. In this context, the decay modes $H \rightarrow \tilde{\chi}_1^0 \tilde{\chi}_2^0, \tilde{\chi}_3^0 \tilde{\chi}_4^0, \tilde{\chi}_1^+ \tilde{\chi}_1^-, \tilde{\chi}_2^+ \tilde{\chi}_2^-$ will be suppressed, the dominant ‘ino’ modes will be those which are manifestly mixtures of gaugino and higgsinos, like $H \rightarrow \tilde{\chi}_1^0 \tilde{\chi}_3^0, \tilde{\chi}_2^0 \tilde{\chi}_3^0, \tilde{\chi}_1^+ \tilde{\chi}_2^-$ etc. Depending on the choice of the electroweakino mass parameters, a wide range of possibilities can arise which may lead to interesting phenomenological collider signatures.

In order to obtain a clear picture of the above-mentioned scenario, in Fig.(1) we show the branching fractions of the heavy Higgses H (upper left), A (upper right) and H^\pm (lower) decaying to SM as well as modes involving electroweakinos. To generate the particle spectrum we use **SUSPECT (version 2.43)** [48] while **HDECAY (version 6.41)** [49] has been used to calculate the branching fractions of the heavy Higgses. Here we vary $\tan \beta$ from 5 to 55 with the following choices,

$$\begin{aligned} M_A = 650 \text{ GeV}, \quad M_1 = 500 \text{ GeV}, \quad M_2 = 150 \text{ GeV}, \quad \mu = 300 \text{ GeV}, \\ M_3 = 5 \text{ TeV}, \quad m_{\tilde{Q}_{3l}} = m_{\tilde{t}_R} = m_{\tilde{b}_R} = 5 \text{ TeV}, \\ A_t = -5 \text{ TeV}, \quad A_b = A_\tau = 0. \end{aligned} \quad (2.8)$$

From Fig.(1) it is evident that we find regions¹ with relatively smaller values of $\tan \beta$ where the non-SM decay modes (i.e. ‘ino’ modes) gain dominance over the SM ones. The non-SM branching ratio is calculated by summing all possible ‘ino’ decay modes of the Higgs boson, for example for H they are $H \rightarrow \tilde{\chi}_i^0 \tilde{\chi}_j^0$ ($i, j = 1-4$) and $H \rightarrow \tilde{\chi}_i^+ \tilde{\chi}_j^-$ ($i, j = 1-2$) modes. Note that, in the low $\tan \beta$ region, $H \rightarrow t\bar{t}$ channel is enhanced because of $\cot \beta$ proportionality factor in the $Ht\bar{t}$ coupling. The $H \rightarrow b\bar{b}$ channel dominates in the high $\tan \beta$ region because of the $Hb\bar{b}$ coupling which is directly proportional to $\tan \beta$. The behavior of the $H \rightarrow \tau^+\tau^-$ channel is also same as the $b\bar{b}$ mode. As a result of these dominant SM branching ratios, the decays of the neutral and charged heavy Higgses to neutralino and/or chargino pairs are suppressed at very low and very high $\tan \beta$ regions. We find that, in order to obtain appreciable branching ratios (at least 10% or more) to the non-SM ‘ino’ modes, we are required to focus in the regions with moderate values of $\tan \beta$, say $\tan \beta = 5 - 20$ regime.

¹In this simple-minded scan, we do not impose the updated Higgs constraints and also any low energy physics constraints except the fact the lightest Higgs boson should have a mass between 122 - 128 GeV. In a more dedicated scan, as we discussed in next section, we do consider all these constraints.

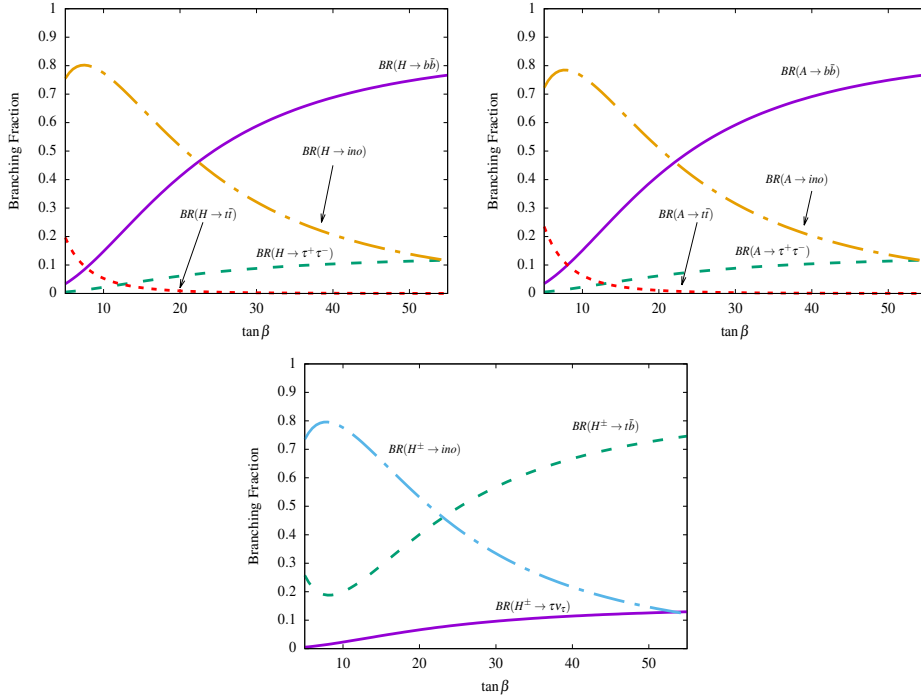


Figure 1: The variation of the heavy Higgs (H, A, H^\pm) branching fractions with $\tan\beta$ for both the SM and non-SM ‘ino’ decay modes. Here the term ‘ino’ refers to the combined chargino and neutralino decay modes of the respective heavy Higgs bosons.

Before we end this section, we would like to briefly discuss how the individual ‘ino’ modes behave with the variation of $\tan\beta$. In Fig.(2), we display the dominant and sub-dominant decay modes of the heavy Higgs bosons H (upper panel) and A (lower panel). The individual ‘ino’ modes of the charged Higgs boson are shown in Fig.(3). From both the figures, Fig.(2) and Fig.(3), it is evident that the dominant $\phi \rightarrow \text{ino}$ ($\phi = H, A, H^\pm$) decay modes are those which are compounded from higgsino and gaugino mixing. For example, the $H, A \rightarrow \tilde{\chi}_1^+ \tilde{\chi}_1^-$ decay mode is highly suppressed as compared to $H, A \rightarrow \tilde{\chi}_1^+ \tilde{\chi}_2^-$ decay mode due to small gaugino-higgsino mixing. Similarly, in the case of $H, A \rightarrow \tilde{\chi}_i^0 \tilde{\chi}_j^0$ ($i, j = 1-4$) decay modes, those channels in which both the neutralinos are either higgsino dominated or gaugino dominated are suppressed as compared to the ones where the neutralinos are manifestly mixed states of gauginos and higgsinos. In summary, from this simple-minded scan we observe that for low to moderate values of $\tan\beta$, the branching ratios of the neutral Higgs H and A to pair of charginos can be as large as 50%, while decay to pair of neutralinos can be around 20%. Now, before we proceed to the next section, we would like to note a few important points. First, we find that these non-SM decay modes (i.e., Higgs decaying to electroweakinos) can be large enough, around 30–40%. However, so far we have not imposed the updated constraints on the various Higgs coupling measurements (usually expressed in terms of the signal strength variables) and the low energy flavour data. Moreover, there exists strong bounds on the masses and couplings of the heavy Higgs bosons from the direct searches. In addition, both the ATLAS and CMS collaborations at the LHC have

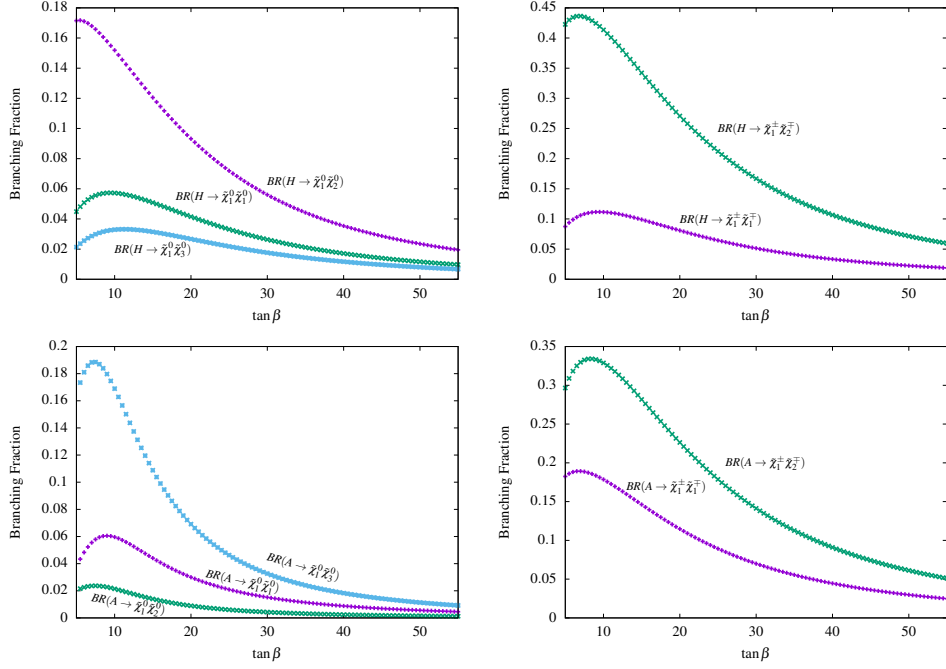


Figure 2: The neutralino and chargino branching ratios of the heavy CP even (upper panel) and CP odd (lower panel) Higgs boson with respect to the variation of $\tan\beta$.

searched for the electroweakinos, strong bounds exist from the LHC run-I and run-II data. In order to calculate the non-SM branching ratios of the heavy Higgses satisfying all the aforementioned collider constraints and low energy flavour data, a dedicated scan involving the MSSM parameters is required to find out the allowed parameter space, which is precisely the goal of the next section.

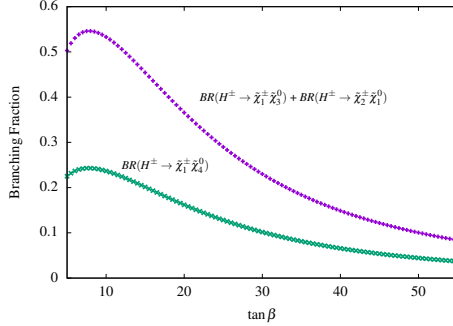


Figure 3: The non-SM branching fractions of the charged Higgs boson with the variation of $\tan\beta$.

2.2 Experimental inputs and Parameter space scan

In this section we describe the parameter space scan along with the details of various experimental constraints considered in our analysis. After the completion of LHC Run-I, both the ATLAS and CMS collaborations at the LHC have published the combined results of 7 and 8 TeV Higgs data [3–5]. At the LHC, the main production mechanism of the Higgs boson (h) is the gluon-gluon fusion (ggF) process, however other sub-dominant production mechanisms are vector boson fusion (VBF), associated production with a W/Z boson (Vh), associated production with a pair of top quarks ($t\bar{t}h$). Both the experimental collaborations have analyzed these processes for different decay modes of the Higgs boson like $h \rightarrow \gamma\gamma$, $h \rightarrow WW^*$, $h \rightarrow ZZ^*$, $h \rightarrow b\bar{b}$, and $h \rightarrow \tau^+\tau^-$ [4, 5]. These results are usually presented in terms of the signal strength variables (μ), defined as the ratio of the production cross section (σ) times the branching ratio (BR) for a specific production and decay mode of the candidate Higgs boson in a given new physics model normalized to the SM predictions, i.e.,

$$\mu_i^f = \frac{\sigma_i \times \text{BR}^f}{(\sigma_i)_{\text{SM}} \times (\text{BR}^f)_{\text{SM}}}, \quad (2.9)$$

where σ_i is the production cross-section corresponding to a new physics model with $i = \text{ggF}, \text{VBF}, \text{VH}$ and $t\bar{t}H$ with H being a generic Higgs boson and $f = \gamma\gamma, ZZ^*, WW^*, b\bar{b}, \tau^+\tau^-$ being the decay modes of the Higgs boson. The subscript ‘‘SM’’ represents the respective SM expectations. These signal strength variables should be measured very precisely as any small but statistically significant deviation from the SM will hint at possible signatures of the beyond SM physics. A combined analysis using 7 and 8 TeV data performed by the ATLAS and CMS collaborations has derived the constraints on the individual signal strength variables as well as in the $\mu_{\text{ggF}+t\bar{t}h}^f, \mu_{\text{VBF}+\text{VH}}^f$ plane through a 10-parameter fit corresponding to five decay modes of the Higgs boson [3]. The above-mentioned study has assumed that μ_V^f and μ_F^f do not change with the variation of the center-of-mass energy from 7 to 8 TeV. In our analysis, the MSSM parameter space obtained after the random scan has been constrained by using the 95% C.L contours in $\mu_{\text{ggF}+t\bar{t}h}^f, \mu_{\text{VBF}+\text{VH}}^f$ plane as presented in Fig.28 of Ref.[3]. We study all five decay modes of the Higgs boson and those points which lie within the 95% C.L. contour are accepted for further analysis.

In addition to the updated Higgs data, we also impose the current flavour physics constraints on $\text{BR}(b \rightarrow s\gamma)$ and $\text{BR}(B_s \rightarrow \mu^+\mu^-)$. In our analysis, we allow 2σ uncertainty on the measurement of these two most stringent rare b-decays with respect to their current measured values $\text{BR}(B_s \rightarrow X_s\gamma) = 3.43 \pm 0.22 \pm 0.21(\text{theo.})$ and $\text{BR}(B_s \rightarrow \mu^+\mu^-) = 3.1 \pm 0.7 \pm 0.31(\text{theo.})$ [50], and assume,

$$\begin{aligned} 2.82 \times 10^{-4} < \text{BR}(B_s \rightarrow X_s\gamma) < 4.04 \times 10^{-4} \\ 1.57 \times 10^{-9} < \text{BR}(B_s \rightarrow \mu^+\mu^-) < 4.63 \times 10^{-9}. \end{aligned} \quad (2.10)$$

We perform a random scan restricting ourselves to the phenomenological MSSM (pMSSM). The parameters that are relevant to our study are mostly associated to the electroweakino sector and Higgs sector of the MSSM, namely the gaugino mass parameters $M_{1,2,3}$, higgsino mass parameter μ , pseudo-scalar mass parameter M_A , $\tan\beta$, the third generation squark trilinear couplings A_t and A_b (trilinear couplings of the sleptons and first two generations squarks are set to zero), third generation squark

and construct several representative models. From Model-B to Model-BWH we vary the parameters M_1 , M_2 and μ by choosing all possible combinations among them (see Table 1-2). The name of each model signifies the nature of lightest electroweakino particle. For example, a name Model-X reflects the fact that the mass parameter ‘X’ is the lightest among all the gaugino and higgsino mass parameters. Similarly, a model name ‘Model-XY’ denotes that both X and Y are varied independently within the specified range, however, with the condition that X is always smaller than Y i.e. $X < Y$. A most general framework where no specific assumptions have been imposed on those parameters is labelled as Model-BWH in Table 2. In all of these representative models, except for Model-BWH, the lightest gaugino/higgsino mass parameter is allowed to vary up to $M_A/2$, as for heavier electroweakinos the decay of the MSSM heavy Higgses to these modes will be kinematically forbidden. The lower values of some of those scanning parameters are determined from existing LEP bounds [54]. Here, the pseudoscalar mass M_A has been varied from 150 GeV to 1 TeV in order to obtain a wide spectrum of the MSSM heavy Higgs boson masses.

Model Name	Parameter varied	Fixed parameters	Mass hierarchy	Range(s) of variation
Model-BH	M_1, μ	$M_2 = 2 \text{ TeV}$	$M_2 \gg \mu > M_1$	$1 \text{ GeV} < M_1 < M_A/2$ $M_1 < \mu < M_A$
Model-HB	M_1, μ	$M_2 = 2 \text{ TeV}$	$M_2 \gg M_1 > \mu$	$100 \text{ GeV} < \mu < M_A/2$ $\mu < M_1 < M_A$
Model-WH	M_2, μ	$M_1 = 2 \text{ TeV}$	$M_1 \gg \mu > M_2$	$100 \text{ GeV} < M_2 < M_A/2$ $M_2 < \mu < M_A$
Model-HW	M_2, μ	$M_1 = 2 \text{ TeV}$	$M_1 \gg M_2 > \mu$	$100 \text{ GeV} < \mu < M_A/2$ $\mu < M_2 < M_A/2$
Model-BWH	M_1, M_2, μ	– –	– –	$100 \text{ GeV} < M_2, \mu < 1000 \text{ GeV}$ $100 \text{ GeV} < M_1 < 1000 \text{ GeV}$

Table 2: Representative models for different possible hierarchy among the gaugino and higgsino mass parameters. In all of these cases the pseudoscalar mass parameter has been varied between $150 \text{ GeV} < M_A < 1000 \text{ GeV}$. A model name ‘Model-XY’ represents the fact that both X and Y have been varied independently within the specified ranges, however, with the condition $X < Y$. The last representative model Model-BWH, however, represents a most general scenario when no specific mass hierarchy among the gaugino and higgsino mass parameters have been imposed, it just denotes the fact that here all the parameters are varied independently.

2.3 SUSY decay of Heavy Higgses and the allowed parameter space

In this section we discuss the results obtained after the parameter space scan for the representative models introduced in the last section and estimate various branching ratios of the heavy Higgses H, A, H^\pm to electroweakinos. Here we would like to remind our readers, these branching fractions

(or say couplings of heavy Higgses to electroweak gaugino/higgsino states) crucially depend on the mixing between electroweak gaugino and higgsino states and, in fact, a almost pure higgsino or gaugino state will have highly suppressed branching ratios with respect to the mixed states. This very feature has been observed for all of those representative models (Model-B - Model-BWH). For example, for Model-B, Model-W, Model-BW and Model-WB, the neutralinos and charginos are almost purely gaugino-like while for Model-H they are purely higgsino-like, and thus offering very negligible amount of mixing between the gaugino and higgsino states. Due to this minuscule mixing, we obtain highly suppressed ($\sim 2\%$) branching fractions for all the heavy Higgses (H, A, H^\pm) decaying to neutralino and chargino states. In Table 3, we summarize the maximum allowed branching ratios for the heavy Higgses summing individual decay modes of a given Higgs boson to different neutralino and chargino states.

	Model-B	Model-W	Model-H	Model-BW	Model-WB
$H \rightarrow \tilde{\chi}_i^0 \tilde{\chi}_j^0$	≤ 0.07	≤ 0.7	≤ 0.65	≤ 1.2	≤ 1.2
$H \rightarrow \tilde{\chi}_k^\pm \tilde{\chi}_\ell^\mp$	~ 0	≤ 1.4	≤ 1.3	≤ 1.3	≤ 1.4
$A \rightarrow \tilde{\chi}_i^0 \tilde{\chi}_j^0$	≤ 0.07	≤ 0.8	≤ 0.7	≤ 1.4	≤ 1.4
$A \rightarrow \tilde{\chi}_k^\pm \tilde{\chi}_\ell^\mp$	~ 0	≤ 1.6	≤ 1.5	≤ 1.6	≤ 1.6
$H^\pm \rightarrow \tilde{\chi}_i^0 \tilde{\chi}_k^\pm$	~ 0	~ 0	≤ 0.25	≤ 1	≤ 1

Table 3: The branching ratios of the heavy Higgses (H, A and H^\pm) to various charginos and neutralinos. The numbers represent the sum of decay modes of the given Higgs boson to all possible neutralino-neutralino, neutralino-chargino and chargino-chargino states for models (B) to (WB) with the indices denote $i, j = 1, 2, 3, 4$ and $k, \ell = 1, 2$.

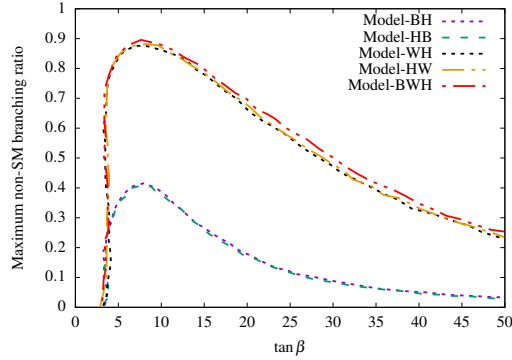


Figure 4: The non-SM branching ratios for Model-BH to Model-BWH (as defined in Table 2) for different values of $\tan\beta$. Here we calculate the maximum possible value of a non-SM ‘ino’ branching fraction among all possible ‘ino’ decay modes of the heavy CP-even Higgs boson (H).

For Model-B to Model-WB (as defined in Table 1) by construction we have negligible amount of gaugino-higgsino mixing and thus the observation of the highly suppressed branching ratios of the heavy Higgses to various neutralino/chargino states is well-understood. Below, however, we allow significant gaugino-higgsino mixing by modifying the parameters and construct five more representative

models, Model-BH to Model-BWH, and estimate the individual non-SM branching ratios. In Fig.(4), we plot the maximum possible value of ‘a’ non-SM branching ratio, out of all possible modes, obtained for a particular value of $\tan\beta$ in the context of all the five representative scenarios Model-BH to Model-BWH (as defined in Table 2). Due to large mixing between higgsinos and gauginos, we find that various ‘ino’ branching ratios can be as large as 40-80%. However it is to be noted that, when both decays are kinematically allowed, the decay of the neutral (both CP even and odd) Higgses to a pair of charginos dominate over the decays to a pair of neutralinos. Moreover, when the wino-higgsino mixing is large compared to bino-higgsino mixing, setting M_2 and μ sufficiently light while M_1 decoupled, the non-SM decay modes can be significantly large. The enhancement is mostly driven by the large BR to the chargino pairs.

We are now in a position to discuss salient features of various representative models in detail. We start with Model-BH and subsequently discuss other models, and also compare the results. In Model-BH, we assume $M_2 \gg \mu > M_1$ with M_2 fixed at 2 TeV, and thus our choice pushes the masses of $\tilde{\chi}_4^0$ and $\tilde{\chi}_2^\pm$ to 2 TeV. One can now expect to see several possible final state signatures involving lighter neutralinos and charginos, for example H/A decaying to $\tilde{\chi}_1^0\tilde{\chi}_2^0, \tilde{\chi}_1^0\tilde{\chi}_3^0, \tilde{\chi}_2^0\tilde{\chi}_3^0, \tilde{\chi}_1^0\tilde{\chi}_1^0, \tilde{\chi}_2^0\tilde{\chi}_2^0, \tilde{\chi}_3^0\tilde{\chi}_3^0$ etc. In Fig.(5), we present branching ratios to these various final state topologies with the variation of $\tan\beta$. In the case when Higgs H/A decays to a pair of neutralinos $H/A \rightarrow \tilde{\chi}_i^0\tilde{\chi}_j^0$ with $i \neq j$, the branching fractions can be as large as 20% each, while for $i = j$ it’s somewhat smaller (for $i = j = 1$, it’s around 10-15%). Decay to a pair of charginos is also possible and, in fact, they can be dominant compared to the neutralino modes depending upon the choices of the parameters. In Fig.(6), we show various branching fractions of the H (left panel) and A (right panel) bosons to a pair of charginos and, as can be clearly seen, these branching ratios are highly suppressed (less than 1%). The reason being negligibly small mixing between the higgsino and wino components, and thereby the lightest chargino is dominantly higgsino-like while heavier one is gaugino-like. The final states of the charged Higgs decay include chargino-neutralino pair and from Fig.(7) we see that these modes can also be sufficiently large for lower values of $\tan\beta$. In fact these branching fractions can go up to $\sim 35\%$ ($\tilde{\chi}_1^\pm\tilde{\chi}_1^0$) and $\sim 20\%$ ($\tilde{\chi}_1^\pm\tilde{\chi}_3^0$) respectively, when the lightest chargino state is higgsino-like and the lightest neutralino is gaugino-like states. On a passing note, large branching ratios to these ‘ino’ modes will lead to interesting collider signatures through cascade decays that can be tested at the ongoing and future runs of LHC.

After having a detailed discussion for Model-BH, let us now interchange the hierarchy of M_1 and μ keeping M_2 decoupled i.e., $M_2 \gg M_1 > \mu$ (Model-HB) and see how the results change. We find that the distributions and various properties are almost same as that of the Model-BH, except the fact that the $\tilde{\chi}_1^0$ and $\tilde{\chi}_2^0$ are now higgsino dominated and $\tilde{\chi}_3^0$ is now bino dominated (for close values of M_1 and μ these states are admixture of bino-higgsino). Hence compared to Model-BH, here the $\text{BR}(H \rightarrow \tilde{\chi}_2^0\tilde{\chi}_3^0)$ and $\text{BR}(A \rightarrow \tilde{\chi}_1^0\tilde{\chi}_3^0)$ dominates and $H/A \rightarrow \tilde{\chi}_1^0\tilde{\chi}_2^0$ has relatively small branching ratios. The charged Higgs branchings to electroweakinos are also in the same ballpark of model-BH. In the low $\tan\beta$ region, the maximum BRs of H^\pm are about 35% for $\tilde{\chi}_1^\pm\tilde{\chi}_3^0$ and 20% for $\tilde{\chi}_1^\pm\tilde{\chi}_1^0$ respectively.

One can also assume a possible hierarchy between the model parameters as $M_1 \gg \mu > M_2$ (Model-WH) or, $M_1 \gg M_2 > \mu$ (Model-HW). The difference between these two scenarios are as follows: in the first case LSP is wino dominated (Model-WH), while in the second case LSP is higgsino

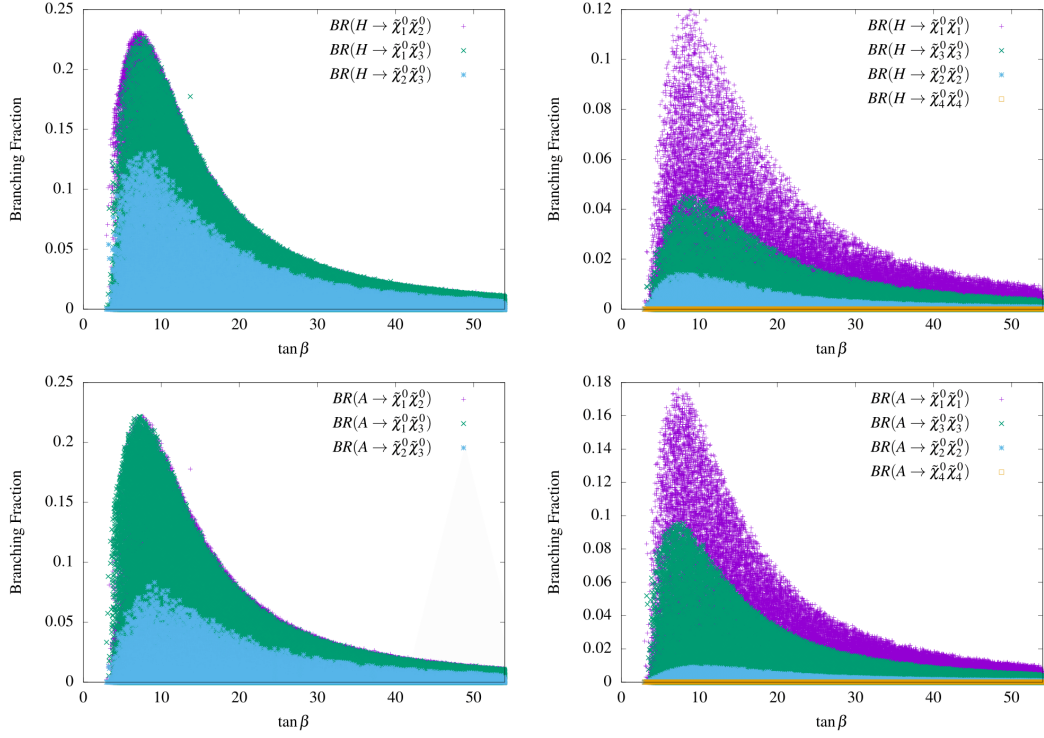


Figure 5: Branching fractions of the heavy Higgs bosons H and A to various neutralinos in the context of Model-BH.

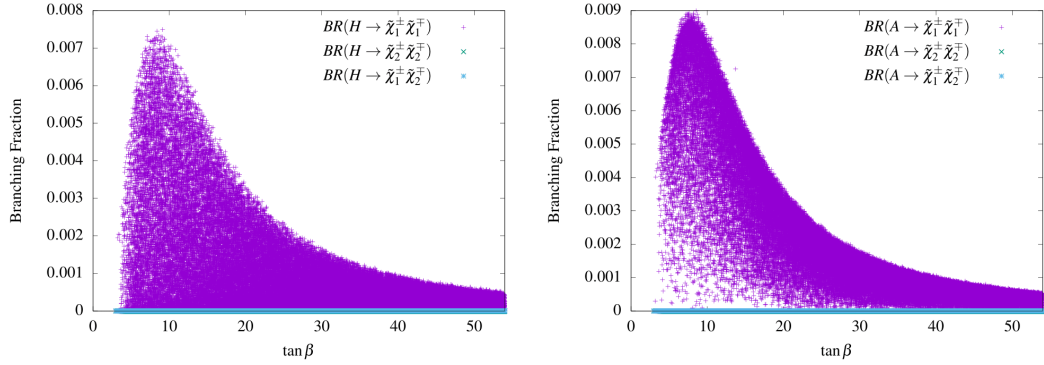


Figure 6: Branching fractions of the heavy Higgs bosons H and A to the charginos in the context of Model-BH.

dominated (Model-HW). We find that, depending on the wino-higgsino mixing and the values of $\tan\beta$, heavy Higgs decaying to a pair of neutralinos and/or charginos can reach up to 10 - 25%. However, due to the presence of light charginos in the particle spectrum and large higgsino-wino mixing, heavy Higgs decaying to a pair of charginos can be as large as 50% for both Model-WH and Model-HW. Moreover, we also find that the charged Higgs decay to a chargino-neutralino pair is also possible (with $BR \sim 25\%$) in the entire region of the parameter space for low to moderate values of $\tan\beta$.

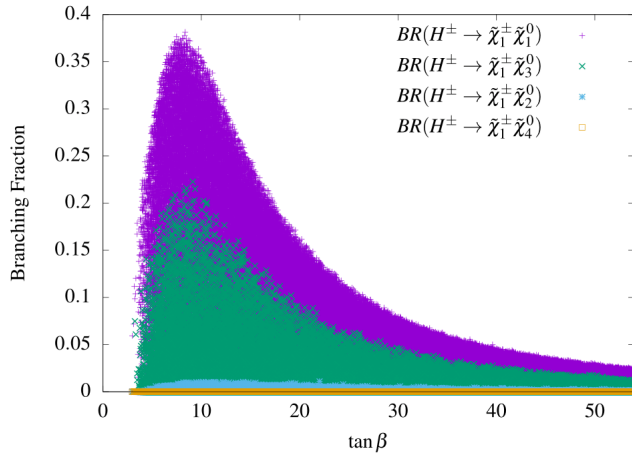


Figure 7: *The decay of the charged Higgs boson H^\pm to chargino-neutralino final states, where we consider Model-BH.*

Given the three free input parameters, M_1 , M_2 and μ , one is not always forced to assume a specific hierarchy between them, instead one can always take a simple-minded approach allowing all of them to vary independently. This is precisely our last representative model, namely Model-BWH where we scan for all possible values of M_1 , M_2 and μ without imposing any hierarchy among them. The added advantage of this kind of choice is many decay modes, which were not kinematically allowed earlier, now will open up and thus will make it phenomenologically richer. For example, the presence of small M_1 , M_2 and μ implies that the decay modes containing $\tilde{\chi}_4^0$ are now accessible in some parts of the parameter space. Again, however, magnitude of the individual decay modes will crucially depend upon the values of M_1 , M_2 and μ . In Fig.(8), we display all the possible decay modes of the heavy neutral and charged Higgs bosons to final states with charginos and neutralinos for Model-BWH. From the distributions one can observe appreciable amount of enhancement in heavy Higgs branching fractions for some of the decay modes which were absent in our earlier constructions (say Model-B to Model-WB). Interestingly, in all of these cases, long cascade decays originating from heavy Higgses decay may result into testable collider signatures, starting from relatively simpler signatures like mono- Z /mono- W /mono- h /dibosons plus \cancel{E}_T signatures, to relatively complex final state topologies consisting of multiple leptons, jets and \cancel{E}_T .

For rest of our analysis, we consider those benchmark models where these heavy Higgses have appreciable amount of branching fractions to charginos and neutralinos, and thus we restrict ourselves within Model-BH to Model-BWH. However, before we advance towards the detailed collider analysis, we would like to remind our readers that there exists avalanche of studies where both the ATLAS and CMS collaborations at the LHC have searched for heavy scalar resonances through different final state signatures. Moreover, direct searches for the electroweakinos have also been performed at the LHC. However, it is difficult to incorporate all these LHC constraints into our parameter space scan. Thus, in order to enliven our analysis, we choose few representative benchmark points which are allowed by the current LHC data and then perform the detailed collider analysis.

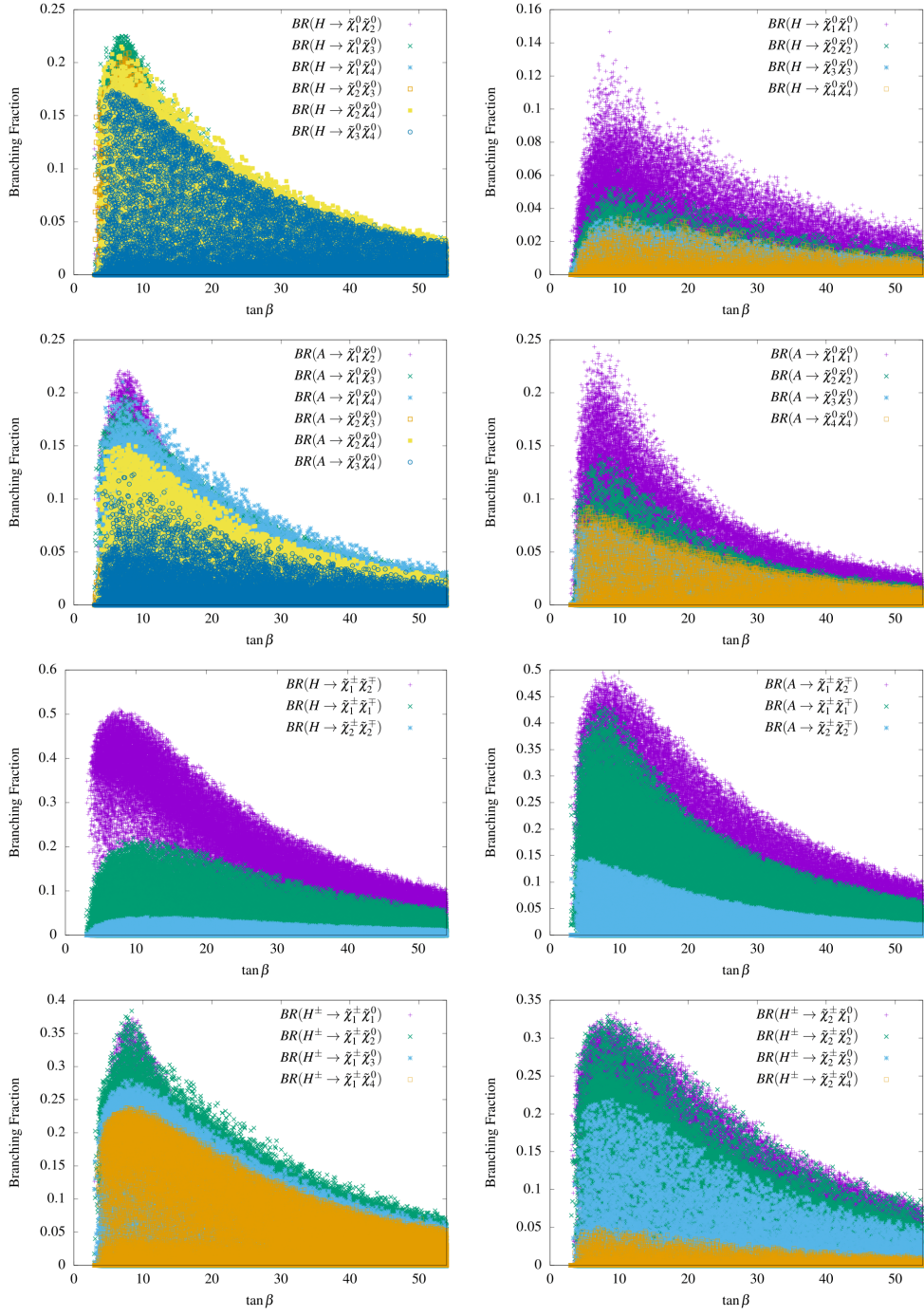


Figure 8: Branching ratios for heavy Higgses (neutral and charged) decaying to various chargino and neutralino final states in the context of Model-BWH.

2.4 Current LHC bounds for heavy Higgs sector and electroweakinos

In this section we summarize the relevant LHC constraints originating mainly from the LHC run-I data and also a few from the early 13 TeV run-II data. We start by discussing the current bounds on the masses and branching ratios of the heavy neutral and charged Higgs bosons obtained by the ATLAS and CMS collaborations for various possible final states, and then proceed to outline the present constraints on the electroweakinos from the run-I data.

2.4.1 Search for H with $\gamma\gamma$ final states

Di-photon invariant mass distribution can be a useful probe to search for the additional Higgses. Both ATLAS and CMS collaboration have looked for scalar particles decaying via narrow resonances into two photon final state using the run-I data [11, 12]. The ATLAS (CMS) collaboration has performed the study using 20.3 (19.7) fb^{-1} data in the mass range 65 - 600 (150 - 850) GeV and no significant excess over the SM background has been observed. The results have been presented as 95% C.L upper limits on the production cross-section times branching ratio into pair of photons i.e., limit on the quantity $\sigma \times \text{Br}(H \rightarrow \gamma\gamma)$. For example, the upper limit² on $\sigma \times \text{Br}(H \rightarrow \gamma\gamma)$ for a heavy Higgs with mass $M_H = 600$ GeV as obtained by the ATLAS is around 1 fb [11].

Recently, both the ATLAS and CMS collaborations have reported an excess in the di-photon invariant mass distribution around 750 GeV with the early 13 TeV data [55, 56]. The local significance of the excess observed by CMS is approximately 3.4σ combining 8 TeV 19.7 fb^{-1} data and 13 TeV 3.2 fb^{-1} data [56]. ATLAS has also observed the excess with local significance 3.9σ for about 50 GeV decay width of the heavy resonance [55]. In our work, we use the 95% C.L upper limits on the production cross section times branching ratio for different choices of heavy resonance masses as derived by both the experimental collaborations.

2.4.2 Search for H with WW final states

Search for a high-mass Higgs boson in the $H \rightarrow WW \rightarrow \ell\nu\ell\nu$ and $H \rightarrow WW \rightarrow \ell\nu qq$ decay channels has been performed by the ATLAS and CMS collaborations using the LHC run-I data [13, 14]. The absence of an evidence of a signal, upper limits on $\sigma \times \text{Br}(H \rightarrow WW)$ as a function of m_H are reported for different possible choices of the width (Γ_H) of the Higgs boson. The ATLAS study has been performed using 20.3 fb^{-1} data in the mass range 200 - 1500 GeV [13] with 8 TeV data. CMS has also performed the same analysis using the complete data set (5.1 + 19.7 fb^{-1}) collected at $\sqrt{s} = 7$ & 8 TeV data in the mass range $145 < m_H < 1000$ GeV [14]. Here we would like to note that as we proceed near the alignment limit [57] (i.e. $(\beta - \alpha) \sim \frac{\pi}{2}$ with α being the Higgs mixing angle), $\text{BR}(H \rightarrow WW)$ become highly suppressed and then bound on $\sigma \times \text{Br}(H \rightarrow WW)$ become less significant for most of the MSSM parameter space (see Fig 7b of Ref [58] for more details). The ATLAS collaboration has also looked for a heavy neutral scalar particle decaying into pair of W bosons, and placed upper limits on the $\sigma \times \text{Br}(H \rightarrow WW)$ as a function of m_H in the entire mass range of 600 GeV to 3 TeV using the LHC run-II data with $\mathcal{L} = 3.2 \text{ fb}^{-1}$ luminosity [59].

²Note that, ATLAS has obtained upper limit on fiducial cross-section (σ_{fid}) times branching ratio, where σ_{fid} includes an efficiency correction factor [11].

2.4.3 Search for H with ZZ final states

Searches for additional Higgses in the ZZ channel have also been reported by the ATLAS and CMS collaborations [14, 15, 60]. The analysis by the ATLAS with 20.3 fb^{-1} of 8 TeV data focuses on the four final state topologies: $H \rightarrow ZZ \rightarrow \ell^+\ell^-\ell^+\ell^-$, $\ell^+\ell^-\nu\bar{\nu}$, $\ell^+\ell^-q\bar{q}$, $\nu\bar{\nu}q\bar{q}$ in the mass range 140 - 1000 GeV [15]. It is needless to mention that better tagging efficiency leads to 4ℓ being the most sensitive channel. In absence of any significant excess 95% C.L upper limit on $\sigma \times \text{Br}(H \rightarrow ZZ)$ for the two production modes of the Higgs boson (ggF and VBF) are obtained by combining all the four search channels with the narrow width approximation.

The same topology has been searched by the CMS collaboration using $(5.1 + 19.7 \text{ fb}^{-1})$ data collected at $\sqrt{s} = 7$ & 8 TeV LHC run focusing in the mass range $145 < m_H < 1000$ GeV [14]. The 95% C.L exclusion limits for different final states are also presented. Recently the ATLAS collaboration has performed a search for heavy Higgs with $H \rightarrow ZZ \rightarrow \ell^+\ell^-q\bar{q}$ final state using 3.2 fb^{-1} run-II data. Non-observation of signal leads to 95% C.L limits in $\sigma \times \text{BR}$ in the entire mass range 300 - 1000 GeV [60].

2.4.4 Search for H with hh final states

The heavy Higgs decay to pair of SM Higgses $H \rightarrow hh$ is significant only in the low $\tan\beta$ (≤ 10) and low to moderate values of $M_A \leq 400$ GeV. At higher values of M_A and low values of $\tan\beta$, the $H \rightarrow t\bar{t}$ channel dominates, thereby all other decay modes get highly suppressed. Depending on the choice of the model parameters, production cross section of single CP even Higgs can be up to two orders of magnitude larger compared to the direct hh production (see Table 1 of Ref.[61]) and it can also have non-trivial effects on the self-coupling measurement of the 125 GeV Higgs [61]. The search for resonant production of a pair of SM Higgs has been done by both the ATLAS and CMS collaborations with 8 TeV data assuming various final state topologies like $b\bar{b}b\bar{b}$ [16, 17], $b\bar{b}\gamma\gamma$ [18, 19], $b\bar{b}\tau\tau$ [20] and $WW\gamma\gamma$ [20]. In fact, in Ref.[20], ATLAS has combined the results for the four above mentioned channels and presented the observed and expected 95% C.L upper limits on $\sigma \times \text{Br}(H \rightarrow hh)$ at $\sqrt{s} = 8$ TeV (see Fig.6 of Ref.[20]). Among the four decay modes, $hh \rightarrow b\bar{b}b\bar{b}$ dominates because of large branching ratio of $h \rightarrow b\bar{b}$. However, the reconstruction of the $b\bar{b}b\bar{b}$ final state presents a formidable complexity because of the large QCD multi-jet background. Thus, less dominant modes like $b\bar{b}\gamma\gamma$ channel become the most sensitive in low and relatively heavy (500 GeV) mass region, as it has comparatively less background and better mass resolution. The CMS collaboration has investigated both the channels, $H \rightarrow hh \rightarrow b\bar{b}b\bar{b}$ and $H \rightarrow hh \rightarrow b\bar{b}\gamma\gamma$, for the mass range $260 \text{ GeV} \leq M_H \leq 1.1$ TeV using LHC-8 data [17, 19]. The ATLAS analyses focused for two different mass regions, for $b\bar{b}b\bar{b}$ they restrict themselves in 500 - 1500 GeV, while for $b\bar{b}\gamma\gamma$ they target the 260 - 500 GeV mass regime [16, 18]. In absence of signal events, both ATLAS and CMS have put 95% C.L upper limits on the production cross section times branching fraction of the heavy resonance for different mass range.

2.4.5 Search for H/A with $\tau^+\tau^-$ final states

The search analysis with $H/A \rightarrow \tau^+\tau^-$ is one of the most important and most promising channels to constrain the MSSM parameter space. The LHC run-I data has already severely constrained the

MSSM parameter space with large to moderate values of $\tan\beta$, say $\gtrsim 15$ using $H \rightarrow \tau^+\tau^-$ channel. The reason why regions with large values of $\tan\beta$ are excluded is primarily because of the heavy Higgs H, A coupling with the SM fermions. For example, the coupling of H, A with down (up) type fermions b, τ (t) increases (decreases) with $\tan\beta$ and thus the dominant production modes of H/A , mainly ggF and associated production with $b\bar{b}$, are primarily controlled by $\tan\beta$. Both the ATLAS and CMS collaborations have looked for signatures of H/A produced via ggF and $b\bar{b}\Phi$ ($\Phi = H, A$) processes with Higgs decaying to $\tau^+\tau^-$ [23, 24] with LHC-8 data. Non-observation of significant excess over the SM backgrounds results into model-independent 95% C.L upper limits on $\sigma \times \text{BR}(\Phi \rightarrow \tau^+\tau^-)$ for different values of M_Φ with $\Phi = H/A$ at 95 % C.L.

Recent results from the ATLAS (CMS) experiment has been reported with final states containing tau pair using the data recorded during 2015 at a centre of mass energy of 13 TeV with $\mathcal{L} = 3.2$ (2.3) fb^{-1} [62, 63]. Both the collaborations have seen a very good agreement between the data and the SM backgrounds. As a result of this agreement 95% C.L. upper limits on the production cross section times branching fraction has been placed. Now, if one translates these experimental upper bounds in terms of the model parameters, say for MSSM in $M_A - \tan\beta$ plane, and compare the run-II data with the existing run-I data, one can clearly observe appreciable improvement in run-II data for regions with $M_A > 700$ GeV while in rest of the parameter space run-I and run-II are already comparable.

2.4.6 Search for A with Zh final states

The decay of pseudoscalar boson A to Zh is kinematically allowed and become appreciable with M_A below the $t\bar{t}$ threshold (i.e., < 350 GeV) and very low values of $\tan\beta$ (< 10). Both the ATLAS and CMS collaborations have investigated this final state topology with h decaying to $b\bar{b}$ (ATLAS has also analyzed $h \rightarrow \tau\tau$ mode [21]) and Z boson into a pair of oppositely charged leptons (electrons or muons) with 8 TeV data [21, 22]. Similar sort of analysis has also been looked at recently by the ATLAS collaboration with 3.2 fb^{-1} run-II data [64]. From all of these analyses, non observation of any signal of A boson leads to an upper limit on the production cross section times branching ratio for a wide range of pseudoscalar masses.

2.4.7 Search for H^\pm with $\tau\nu$ and $t\bar{b}$ final states

The observation of a charged Higgs boson signal is one of the smoking gun signatures of physics beyond the SM. From the direct searches at the Large Electron-Positron (LEP) collider, charged Higgs masses have to be greater than around 80 GeV [54]. At the LHC, the search strategies of charged Higgses crucially depend on its mass, in other words, when the charged Higgs is light ($M_{H^\pm} < M_{\text{top}}$) then it is primarily produced from the $t\bar{t}$ process and decays into $\tau\nu_\tau$ final states. However, for heavy H^\pm ($M_{H^\pm} > M_{\text{top}}$), they are mainly produced in associated production with top and bottom quarks i.e., $pp \rightarrow tbH^\pm$.

Both the ATLAS and CMS collaborations have searched for light H^\pm , produced through $t\bar{t}$ processes and decaying to $c\bar{s}$ and $\tau\nu_\tau$ final states with LHC-8 data [25–27]. Search for heavy charged Higgs via $H^\pm \rightarrow t\bar{b}$ channel with multi b -jets in the final states has also been studied [26, 28]. Again, non observation of any excess over the SM predictions leads to 95% C.L. exclusion limits on the pro-

duction cross-section times branching ratios for different values of M_{H^\pm} . From the exclusion limits, we find that regions with very high $\tan\beta$ (> 20 - 25) are only severely constrained for relatively large values of charged Higgs mass. Recently ATLAS collaboration has presented the early run-II results for H^\pm decaying into $\tau\nu$ final states with $\mathcal{L} = 3.2 \text{ fb}^{-1}$ dataset corresponding to $\sqrt{s} = 13 \text{ TeV}$ [65]. However, similar to run-I data, they have again placed 95% C.L. upper limits on $\sigma \times \text{Br}$ which are very much similar to the existing 8 TeV bounds.

2.4.8 Current LHC bounds for electroweakinos

The relatively smaller production cross section of the electroweak sparticles, namely charginos, neutralinos and sleptons, results into comparatively weaker bounds on their masses and couplings compared to the colored SUSY particles. However with the 8 TeV data, the ATLAS and CMS collaborations have already placed strong constraints on the masses/couplings through direct searches of the electroweakinos [66–72]. The mass bounds obtained by the ATLAS and CMS are mostly based on simplified SUSY scenarios. However we know that these bounds crucially depend on the hierarchy between the slepton and the gaugino masses, composition of the electroweakinos and most importantly on their branching ratios³. Majority of these searches assume a bino-like LSP, while the second lightest neutralino ($\tilde{\chi}_2^0$) and the lighter chargino ($\tilde{\chi}_1^\pm$) to be purely wino-like [66–72]. In fact, the most significant bound is obtained from the $\tilde{\chi}_1^\pm \tilde{\chi}_2^0$ pair production process with trilepton plus missing energy (\cancel{E}_T) signature [66, 72].

In our work we assume sleptons to be sufficiently heavy (masses around 3 TeV), and thus the electroweakinos mainly decay via W, Z, h bosons. With decoupled scenario the limits become much weaker compared to the scenarios with intermediate lighter sleptons⁴. For wino-dominated $\tilde{\chi}_1^\pm$ and $\tilde{\chi}_2^0$ decaying 100% to $\tilde{\chi}_1^\pm \rightarrow \tilde{\chi}_1^0 W^\pm$ and $\tilde{\chi}_2^0 \rightarrow \tilde{\chi}_1^0 Z$ and with decoupled sleptons, the mass limits on charginos obtained by the ATLAS and CMS collaborations are 350 GeV for a massless LSP and 305 GeV for $m_{\tilde{\chi}_1^0} = 125 \text{ GeV}$. However, note that, the limits entirely vanish for $m_{\tilde{\chi}_1^0} > 125 \text{ GeV}$. The exclusion limits are weakest when $\tilde{\chi}_2^0$ decays via the *spoiler* mode ($h\tilde{\chi}_1^0$) [69, 70, 72]. Moreover, degenerate chargino-neutralino masses up to 148 GeV are excluded for LSP masses up to 20 GeV when the decay modes of neutralinos involve a Higgs boson through trilepton + \cancel{E}_T signature. Furthermore, the ATLAS collaboration has also presented the electroweakino searches with $1\ell + 2b$ and $1\ell + 2\gamma$ ($\ell = e, \mu$) final states [69] for simplified models with the assumption $\text{BR}(\tilde{\chi}_2^0 \rightarrow \tilde{\chi}_1^0 h) = 100\%$. The limit obtained from $1\ell + 2\gamma$ ($\ell = e, \mu$) channel is little bit stronger than the trilepton bounds. However, it is to be remembered that the sharing of the branching ratios between $\tilde{\chi}_1^0 h$ and $\tilde{\chi}_1^0 Z$ can modify the exclusion limits considerably, for details we refer a recent study [74].

In this work, we consider the present LHC constraints⁵ on the electroweakinos via the $3\ell + \cancel{E}_T$, $1\ell + 2b + \cancel{E}_T$ and $1\ell + 2\gamma + \cancel{E}_T$ ($\ell = e, \mu$) channels obtained by the ATLAS collaborations with the LHC-8 data. To study⁶ the impact of these constraints on our parameter space, we first calculate

³In most of the analysis, LHC collaborations assume 100% branching ratio into one particular decay mode.

⁴In a recent study [73] it has been shown that LHC constraints are significantly weaker in models with higgsino dominated $\tilde{\chi}_1^\pm, \tilde{\chi}_2^0$ and $\tilde{\chi}_3^0$; compared to the scenarios studied by the LHC collaborations with wino-dominated $\tilde{\chi}_1^\pm, \tilde{\chi}_2^0$.

⁵We do not consider the CMS constraints as we find them comparable with that of ATLAS collaboration.

⁶For details about the implementation and validation of our analysis, we refer [74].

the signal and background efficiencies for some representative benchmark points (see next section), and then using the NLO production cross-sections as obtained from the PROSPINO [75] we estimate the effective cross sections and then make sure that our numbers lie below the 95% C.L. upper limits already presented by the ATLAS collaboration in the three above-mentioned channels.

3 Search strategies and Future limits

From the previous section, we find that the branching fraction of the heavy Higgses to non-SM ‘ino’ pairs can be significantly large. Moreover, the charginos and neutralinos produced from the decay of heavy Higgses can themselves also undergo long cascade decays depending upon the choice of MSSM parameters. As such, a myriad of possible cascade decay modes are possible corresponding to various final state topologies. For example, one can have a very simple cascade decay of the form $H \rightarrow \tilde{\chi}_2^0 \tilde{\chi}_1^0$, $\tilde{\chi}_2^0 \rightarrow Z/h \tilde{\chi}_1^0$, resulting in a mono-Z/h + \cancel{E}_T final state or, $H^\pm \rightarrow \tilde{\chi}_1^\pm \tilde{\chi}_1^0$, $\tilde{\chi}_1^\pm \rightarrow W^\pm \tilde{\chi}_1^0$, resulting in mono-W + \cancel{E}_T final state. However, one can also encounter relatively complex cascade decays with multiple decay chains in between, for example, $H \rightarrow \tilde{\chi}_2^0 \tilde{\chi}_3^0$, $\tilde{\chi}_2^0 \rightarrow Z \tilde{\chi}_1^0$, $\tilde{\chi}_3^0 \rightarrow W^\pm \tilde{\chi}_1^\pm$, which may eventually lead to final states with multiple leptons and jets along with large missing energy. As we have already mentioned, one can have a significant branching fraction for these cascade decays by making judicious choices of the parameters. Proper understanding of these cascade decays with various possible final state topologies can be considered as a direct probe of the MSSM Higgs sector. In this work, we perform a detailed collider analysis of the MSSM heavy Higgses focusing the mono-X + \cancel{E}_T ($X = W, Z$) and tripleton + \cancel{E}_T channels in the context of 14 TeV high luminosity run of LHC. Here we assume that the SM gauge bosons W/Z decay leptonically i.e., $W \rightarrow \ell \nu$ and $Z \rightarrow \ell \ell$ with $\ell = e, \mu$, in order to reduce the SM backgrounds significantly. The hadronic decay modes might also be important, however, we do not consider them in this work. Searches through mono-Higgs plus \cancel{E}_T also exist literature, for details we refer [76].

3.1 Benchmark points

To present the collider analysis we choose four optimized benchmark points (BP-1 to BP-4) suitable for the above-mentioned three search strategies. All the model parameters, masses of heavy Higgses and electroweakinos and the relevant branching ratios are summarized in Table 4. For all the four benchmark points, heavy Higgs masses lie in the mass range of 500 - 700 GeV. The first two benchmark points, BP-1 and BP-2, are optimized for the mono-Z + \cancel{E}_T searches, where the lightest chargino and the second/third lightest neutralinos are higgsino dominated and LSP is bino dominated. In BP-1, $\text{BR}(\tilde{\chi}_2^0, \tilde{\chi}_3^0 \rightarrow Z \tilde{\chi}_1^0) = 100\%$ and the total contribution coming from H/A to $\tilde{\chi}_2^0 \tilde{\chi}_1^0, \tilde{\chi}_3^0 \tilde{\chi}_1^0$ are about 30%, while in BP-2, the decay modes $\tilde{\chi}_2^0, \tilde{\chi}_3^0 \rightarrow h \tilde{\chi}_1^0$ open up and consequently the branching ratios to $Z \tilde{\chi}_1^0$ get reduced. Our third benchmark point, BP-3, is optimized for the mono-W + \cancel{E}_T searches where LSP is mixture of substantial wino and higgsino components while $\tilde{\chi}_2^0, \tilde{\chi}_3^0$ are higgsino dominated. Here $\tilde{\chi}_1^\pm$ is primarily wino but has significant higgsino component. In Table 4, all the relevant branching ratios of $H/A \rightarrow \chi_1^\pm \chi_2^\mp, \tilde{\chi}_1^0 \chi_{2,3}^0$ are summarized. In BP-4, the input parameters M_1, M_2 and μ all are relatively light and close to each others, and hence the charginos and neutralinos are mixed states of

Benchmark Points	Parameters (GeV)	Mass (GeV)	Processes	Branching Fraction
BP-1	$M_A = 591.2, \quad M_1 = 127.1,$ $M_2 = 900, \quad \mu = 237.2,$ $\tan \beta = 15, \quad A_t = 1890,$ $m_{\tilde{Q}_{3l}} = 4160, \quad m_{\tilde{t}_R} = 6520,$ $m_{\tilde{b}_R} = 2280, \quad A_b = A_\tau = 0$ $M_3 = 2960$	$M_{\chi_1^0} = 119.7$ $M_{\chi_2^0} = 241.8$ $M_{\chi_3^0} = 241.8$ $M_{\chi_4^0} = 907.4$ $M_{\chi_{1\pm}} = 234.3$ $M_{\chi_{2\pm}} = 907.4$ $M_H = 591.3$ $M_{H^\pm} = 596.8$	$H \rightarrow \chi_2^0 \chi_1^0$ $H \rightarrow \chi_3^0 \chi_1^0$ $A \rightarrow \chi_2^0 \chi_1^0$ $A \rightarrow \chi_3^0 \chi_1^0$ $\chi_2^0 \rightarrow Z \chi_1^0$ $\chi_3^0 \rightarrow Z \chi_1^0$	4.58% 10.14% 9.23% 4.65% 100% 100%
BP-2	$M_A = 550, \quad M_1 = 80,$ $M_2 = 900, \quad \mu = 350,$ $\tan \beta = 8.5, \quad A_t = 3770,$ $m_{\tilde{Q}_{3l}} = 3380, \quad m_{\tilde{t}_R} = 9040,$ $m_{\tilde{b}_R} = 2820, \quad A_b = A_\tau = 0$ $M_3 = 8900$	$M_{\chi_1^0} = 77.2$ $M_{\chi_2^0} = 347.8$ $M_{\chi_3^0} = 353.6$ $M_{\chi_4^0} = 908.5$ $M_{\chi_{1\pm}} = 345.1$ $M_{\chi_{2\pm}} = 908.5$ $M_H = 550.6$ $M_{H^\pm} = 556.0$	$H \rightarrow \chi_2^0 \chi_1^0$ $H \rightarrow \chi_3^0 \chi_1^0$ $A \rightarrow \chi_2^0 \chi_1^0$ $A \rightarrow \chi_3^0 \chi_1^0$ $\chi_2^0 \rightarrow Z \chi_1^0$ $\chi_3^0 \rightarrow Z \chi_1^0$	4.82% 13.93% 14.14% 3.89% 24.25% 83.56%
BP-3	$M_A = 600, \quad M_1 = 950,$ $M_2 = 178.2, \quad \mu = 286.1,$ $\tan \beta = 21, \quad A_t = 4320,$ $m_{\tilde{Q}_{3l}} = 3370, \quad m_{\tilde{t}_R} = 4230,$ $m_{\tilde{b}_R} = 5330, \quad A_b = A_\tau = 0$ $M_3 = 7100$	$M_{\chi_1^0} = 158.2$ $M_{\chi_2^0} = 292.7$ $M_{\chi_3^0} = 310.3$ $M_{\chi_4^0} = 952.3$ $M_{\chi_{1\pm}} = 159.0$ $M_{\chi_{2\pm}} = 316.8$ $M_H = 600.0$ $M_{H^\pm} = 605.5$	$H \rightarrow \chi_1^\pm \chi_2^\mp$ $A \rightarrow \chi_1^\pm \chi_2^\mp$ $\chi_2^\pm \rightarrow W^\pm \chi_1^0$ $H \rightarrow \chi_1^0 \chi_2^0$ $H \rightarrow \chi_1^0 \chi_3^0$ $A \rightarrow \chi_1^0 \chi_2^0$ $A \rightarrow \chi_1^0 \chi_3^0$ $\chi_2^0 \rightarrow \chi_1^\pm W^\mp$ $\chi_3^0 \rightarrow \chi_1^\pm W^\mp$	23.39% 16.70% 43.48% 8.30% 1.30% 3.05% 4.10% 73.32% 81.06%
BP-4	$M_A = 657.5, \quad M_1 = 159.5,$ $M_2 = 337.2, \quad \mu = 236.6,$ $\tan \beta = 23, \quad A_t = 1290,$ $m_{\tilde{Q}_{3l}} = 9590, \quad m_{\tilde{t}_R} = 1920,$ $m_{\tilde{b}_R} = 2600, \quad A_b = A_\tau = 0$ $M_3 = 6180$	$M_{\chi_1^0} = 145.5$ $M_{\chi_2^0} = 230.7$ $M_{\chi_3^0} = 248.9$ $M_{\chi_4^0} = 387.6$ $M_{\chi_{1\pm}} = 221.4$ $M_{\chi_{2\pm}} = 387.3$ $M_H = 657.5$ $M_{H^\pm} = 662.4$	$H \rightarrow \chi_1^\pm \chi_2^\mp$ $A \rightarrow \chi_1^\pm \chi_2^\mp$ $\chi_2^\pm \rightarrow W^\pm \chi_3^0$ $\chi_3^0 \rightarrow Z \chi_1^0$ $H \rightarrow \chi_3^0 \chi_4^0$ $A \rightarrow \chi_3^0 \chi_4^0$ $\chi_4^0 \rightarrow W^\pm \chi_1^\pm$	28.971% 15.8% 21.85% 100% 8.89% 0.39% 67.78%

Table 4: Input parameters, masses of heavy Higgses and electroweakinos, and branching fraction of relevant processes for benchmark points. Here all the input mass parameters and output masses are in GeV.

bino, wino and higgsino states. Several possible long cascade decays of these electroweakinos (see last column of Table 4) leads to final state topologies with trileptons plus missing energy.

	Production Cross-section in fb							
	8 TeV				13(14) TeV			
	BP-1	BP-2	BP-3	BP-4	BP-1	BP-2	BP-3	BP-4
H	65	41	114	21	290(356)	171(207)	517(635)	100(129)
A	70	51	119	24	311(380)	208(252)	534(657)	114(140)
H $^\pm$	1.1	0.8	1.9	0.4	7.3(9.4)	5.12(6.5)	12.9(16.8)	3.2(4.2)

Table 5: Production cross-sections of the heavy Higgses H, A and H^\pm for $\sqrt{s} = 8, 13$ and 14 TeV. Higgses are predominantly produced through ggF process. Charged Higgs production cross-sections are small, so we ignore them in our analysis.

In Table 5 we present the production cross-sections of the MSSM heavy Higgses H, A and H^\pm for center-of-mass energies $\sqrt{s} = 8, 13$ and 14 TeV. We assume that these Higgses are predominantly produced via the gluon-gluon fusion process. From the last row of Table 5, it is clear that the charged Higgs production cross-sections are much smaller compared to the H, A cross-sections, and hence we ignore them in rest of our analysis. Once we know the cross-sections of these Higgses and also branching ratios to different decay modes, we can calculate the quantity $\sigma \times \text{BR}$ for all the benchmark points and then compare our results with the present experimental bounds. In Table 6, we display the observed 95% C.L. upper limits on the production cross-section times branching ratios for the heavy Higgses obtained by the ATLAS and CMS collaborations using the run-I and run-II data. We also quote the predictions for a given decay mode associated to all the four benchmark points. Here, we consider the following Higgs decay modes: $H/A \rightarrow \gamma\gamma, WW, ZZ, hh, \tau\tau$; $A \rightarrow Zh$; $H^\pm \rightarrow \tau\nu, t\bar{b}$. The quantity $\sigma \times \text{Br}(H/A \rightarrow XX)_{ATLAS/CMS}^{UL}$ denotes the 95% C.L. upper limit on the production cross-section times branching ratios observed by the ATLAS/CMS collaborations, and $\sigma \times \text{Br}(H/A \rightarrow XX)$ is the same but for our representative benchmark points for a generic heavy Higgs decay $H/A \rightarrow XX$ channel. We observe that, in most of the cases, the limits from LHC run-I data is more stringent than the early run-II data and, except for the $H/A \rightarrow \tau\tau$ channel, the observed upper limits are few order of magnitude smaller than the predicted values for the benchmark points.

In addition to the heavy Higgs direct search bounds, we also consider the limits obtained from the direct searches of the charginos and neutralinos at the LHC. Both the ATLAS and CMS collaboration have searched for these electroweakinos, and placed upper limits on the production cross-sections. We find that the limits of ATLAS and CMS collaborations are comparable, and so in our analysis we use the ATLAS limits only. All the benchmark points, BP-1 to BP-4, possess significant gaugino-higgsino mixing which leads to sizeable modifications in electroweakino pair production cross-sections. We calculate all the dominant chargino-neutralino pair production cross-sections (see Table 7) and then following the ATLAS analysis [66, 69], we estimate the cut efficiencies for the three final state topologies $3\ell + \cancel{E}_T, 1\ell + 2b + \cancel{E}_T$ and $1\ell + 2\gamma + \cancel{E}_T$ ($\ell = e, \mu$). In Table 7, we present the observed 95% C.L. upper limits on the number of BSM signal events, $N_{BSM}^{Obs. UL}$, by the ATLAS collaborations for

Modes	$\sqrt{s} = 8 \text{ TeV}(\text{fb})$				$\sqrt{s} = 13 \text{ TeV}(\text{fb})$			
	BP-1	BP-2	BP-3	BP-4	BP-1	BP-2	BP-3	BP-4
$\sigma \times \text{Br}(H/A \rightarrow \gamma\gamma)_{ATLAS}^{UL}$ [11, 55]	0.9	1.8	0.6	-	3.0	3.6	3.3	2.0
$\sigma \times \text{Br}(H/A \rightarrow \gamma\gamma)_{CMS}^{UL}$ [12, 56]	1.4	1.2	1.0	0.5	5.1	4.6	3.7	1.3
$\sigma \times \text{Br}(H/A \rightarrow \gamma\gamma)$	$\sim 10^{-6}$	$\sim 10^{-4}$	$\sim 10^{-4}$	$\sim 10^{-6}$	$\sim 10^{-4}$	$\sim 10^{-3}$	$\sim 10^{-3}$	$\sim 10^{-4}$
$\sigma \times \text{Br}(H \rightarrow WW)_{ATLAS}^{UL}$ [13, 59]	242.8	308.6	229.3	186.5	570.7	817.7	543.2	457.8
$\sigma \times \text{Br}(H \rightarrow WW)_{CMS}^{UL}$ [14]	124.99	148.02	121.28	109.65	-	-	-	-
$\sigma \times \text{Br}(H \rightarrow WW)$	0.04	0.18	0.01	0.01	0.18	0.76	0.06	0.06
$\sigma_{ggH} \times \text{Br}(H \rightarrow ZZ)_{ATLAS}^{UL}$ [15, 60]	23.7	30.8	21.2	26.2	329.8	456.4	304.1	195.8
$\sigma_{ggH} \times \text{Br}(H \rightarrow ZZ)$	$\sim 10^{-3}$	0.02	$\sim 10^{-4}$	$\sim 10^{-5}$	$\sim 10^{-3}$	0.11	$\sim 10^{-3}$	$\sim 10^{-3}$
$\sigma \times \text{Br}(H \rightarrow ZZ)_{CMS}^{UL}$ [14]	128.96	140.01	125.32	117.71	-	-	-	-
$\sigma \times \text{Br}(H \rightarrow ZZ)$	0.02	0.09	$\sim 10^{-2}$	$\sim 10^{-3}$	0.09	0.37	0.03	0.03
$\sigma_{ggF} \times \text{Br}(H \rightarrow hh)_{ATLAS}^{UL}$ [20]	87.8	121.1	79.1	42.3	-	-	-	-
$\sigma_{ggF} \times \text{Br}(H \rightarrow hh)$	0.01	0.2	0.002	0.006	0.04	0.78	0.009	0.024
$\sigma \times \text{Br}(H \rightarrow hh \rightarrow \gamma\gamma b\bar{b})_{CMS}^{UL}$ [19]	1.19	1.47	1.13	0.77	-	-	-	-
$\sigma \times \text{Br}(H \rightarrow hh \rightarrow \gamma\gamma b\bar{b})$	$\sim 10^{-4}$	$\sim 10^{-4}$	$\sim 10^{-4}$	$\sim 10^{-4}$	$\sim 10^{-3}$	$\sim 10^{-3}$	$\sim 10^{-3}$	$\sim 10^{-4}$
$\sigma_{gg\phi} \times \text{Br}(\phi \rightarrow \tau\tau)_{ATLAS}^{UL}$ [24, 63]	19.1	21.9	19.0	15.6	112.0	148.3	104.1	83.8
$\sigma_{gg\phi} \times \text{Br}(\phi \rightarrow \tau\tau)_{CMS}^{UL}$ [23, 62]	23.1	29.6	22.4	17.5	85.7	96.5	84.6	75.2
$\sigma_{ggH+ggA} \times \text{Br}(H/A \rightarrow \tau\tau)$	1.46	2.24	1.14	0.31	5.62	8.38	4.44	1.29
$\sigma_{bb\phi} \times \text{Br}(\phi \rightarrow \tau\tau)_{ATLAS}^{UL}$ [24, 63]	19.1	21.9	18.6	14.9	106.7	147.8	97.6	80.1
$\sigma_{bb\phi} \times \text{Br}(\phi \rightarrow \tau\tau)_{CMS}^{UL}$ [23, 62]	22.7	25.7	21.4	20.2	72.8	79.0	71.1	93.4
$\sigma_{bbH+bbA} \times \text{Br}(H/A \rightarrow \tau\tau)$	11.62	3.51	14.97	1.30	52.46	15.15	68.28	6.35
$\sigma \times \text{Br}(A \rightarrow Zh)_{ATLAS}^{UL}$ [21, 64]	41.4	43.1	41.0	26.3	412.6	709.9	365.3	250.3
$\sigma \times \text{Br}(A \rightarrow Zh)_{CMS}^{UL}$ [22]	83.29	131.9	67.0	-	-	-	-	-
$\sigma \times \text{Br}(A \rightarrow Zh)$	0.04	0.2	0.013	0.0062	0.16	0.8	0.06	0.03
$\sigma \times \text{Br}(H^\pm \rightarrow \tau\nu)_{ATLAS}^{UL}$ [27, 65]	11.12	14.48	9.94	8.84	53.4	66.9	50.3	39.2
$\sigma \times \text{Br}(H^\pm \rightarrow \tau\nu)_{CMS}^{UL}$ [26]	26.28	30.31	25.97	-	-	-	-	-
$\sigma \times \text{Br}(H^\pm \rightarrow \tau\nu)$	0.12	0.05	0.14	0.02	0.76	0.33	0.96	0.12
$\sigma \times \text{Br}(H^\pm \rightarrow t\bar{b})_{ATLAS}^{UL}$ [28]	208.7	487.7	238.8	-	-	-	-	-
$\sigma \times \text{Br}(H^\pm \rightarrow t\bar{b})_{CMS}^{UL}$ [26]	137.1	166.1	132.7	-	-	-	-	-
$\sigma \times \text{Br}(H^\pm \rightarrow t\bar{b})$	0.78	0.59	0.89	0.13	5.09	3.69	5.90	0.99

Table 6: Upper limits on the production cross-section times the branching ratios at 95% C.L. for various decay modes obtained by ATLAS and CMS collaborations and the corresponding values for the benchmark points introduced in Table 4.

the most sensitive signal regions for the above-mentioned three channels. In Table 7 we also present the production cross-sections and N_{BSM} for our benchmark points for 8 TeV LHC with $\mathcal{L} = 20.3 \text{ fb}^{-1}$, where the quantity $N_{BSM} = \text{production cross-section} \times \text{efficiency} \times \text{acceptance} \times \text{luminosity}$ for a given channel. From the table, it is evident that the models predictions are much smaller compared to the observed 95% C.L. upper limits, and thus all our benchmark points are consistent with the updated bounds associated to direct searches of the electroweakinos at the LHC.

	BP-1	BP-2	BP-3	BP-4
$\sigma(pp \rightarrow \tilde{\chi}_1^\pm \tilde{\chi}_2^0)$	91.01	18.76	17.75	131.24
$\sigma(pp \rightarrow \tilde{\chi}_1^\pm \tilde{\chi}_3^0)$	95.57	17.77	13.12	85.55
$\sigma(pp \rightarrow \tilde{\chi}_1^\pm \tilde{\chi}_4^0)$	-	-	-	3.32
$\sigma(pp \rightarrow \tilde{\chi}_2^\pm \tilde{\chi}_2^0)$	-	-	29.35	3.61
$\sigma(pp \rightarrow \tilde{\chi}_2^\pm \tilde{\chi}_3^0)$	-	-	39.39	3.93
$\sigma(pp \rightarrow \tilde{\chi}_2^\pm \tilde{\chi}_4^0)$	-	-	-	35.07
σ_{Total}	187.6	36.53	99.61	262.68
N_{BSM} for SR0 τ a-bin16 ($N_{BSM}^{Obs. UL} = 5.2$ [66])	0.93	0.99	0.48	0.65
N_{BSM} for SRlbb-2 ($N_{BSM}^{Obs. UL} = 5.5$ [69])	0	0.76	0.1	0.05
N_{BSM} for SRl $\gamma\gamma$ -1 ($N_{BSM}^{Obs. UL} = 3.6$ [69])	0	0.08	0.05	0.02

Table 7: Here the cross-sections (NLO) are in fb. $N_{BSM}^{Obs. UL}$ stands for Observed upper limits on N_{BSM} at 95 % CL where $N_{BSM} =$ production cross-section \times efficiency \times acceptance \times luminosity.

3.2 Mono-X plus missing energy

Events with a single W/Z boson plus missing transverse energy (\cancel{E}_T) constitute a very clean and distinctive signature in new physics searches at the LHC. This topology has been thoroughly analyzed by both the ATLAS and CMS collaborations, mainly in the context of DM searches. In this paper, we consider two such mono-X + \cancel{E}_T channels, namely mono- Z and mono- W , with both W, Z decaying leptonically ($Z \rightarrow ll, W \rightarrow l\nu, l = e, \mu$) to search for the MSSM heavy Higgses at the LHC.

Below, we discuss the details of the collider analysis for our optimized benchmark points for the above-mentioned mono-X search channels. We use **MadGraph (version 2.3.3)** [77] to generate the background events and **PYTHIA (version 6.428)** [78] for showering and hadronization. The production cross-sections of the heavy Higgses H, A have been calculated using **SusHi (version 1.5.0)** [79], while for the charged Higgs boson H^\pm we use **PYTHIA**. To obtain the particle spectrum we use **SUSPECT** while **SUSYHIT** has been used to calculate the Higgs and SUSY decay widths and branching ratios. The signal events have been generated through gluon-gluon fusion process using **PYTHIA**. Both the signal and background events have been passed through a fast detector simulation using **Delphes3 (version-3.3.2)** [80] using the default ATLAS card.

3.2.1 Mono- Z (leptonic) + \cancel{E}_T channel

We perform a search for the MSSM heavy Higgses in events with a leptonically decaying Z boson ($Z \rightarrow \ell^+ \ell^-, \ell = e, \mu$) produced through cascade decays of the charginos and neutralinos in the context of $\sqrt{s} = 14$ TeV run of LHC with an integrated luminosity of 3000 fb^{-1} . These events also contain significant missing transverse energy coming from the lightest neutralinos. The search strategy reported in [81], which focused on the DM searches, has been followed with suitable modifications

aimed to optimize the signal significance. This analysis has been performed on the first two representative benchmark points, BP-1 and BP-2 (see Table 4). The relevant decay chains giving rise to the above-mentioned final state signature are: $pp \rightarrow H/A$, $H/A \rightarrow \tilde{\chi}_{2,3}^0 \tilde{\chi}_1^0$, $\tilde{\chi}_{2,3}^0 \rightarrow \tilde{\chi}_1^0 Z$.

The events are selected with two same flavour opposite sign (SFOS) isolated leptons (electrons or muons) with p_T greater than 20 GeV. Candidate electrons(muons) are required to be within pseudo-rapidity range $|\eta| < 2.47(2.5)$. For an electron or muon to be isolated, the scalar p_T sum of all stable particles with $p_T > 1$ GeV present within a cone of radius $\Delta R = 0.2$ around the direction of candidate lepton should be less than 10% of p_T of the candidate lepton, where $\Delta R = \sqrt{(\Delta\phi)^2 + (\Delta\eta)^2}$ with ϕ being the azimuthal angle. The azimuthal angle between the dilepton system and \cancel{E}_T direction, $\Delta\phi_{p_T^{\ell\ell}, \cancel{E}_T}$, is required to be greater than 2.5, where $p_T^{\ell\ell}$ is the momentum of the dilepton system. In addition, the absolute value of pseudo-rapidity of the dilepton system, $|\eta_{\ell\ell}|$, must lie within 2.5 and the invariant mass of the SFOS pair is required to be within $M_Z \pm 15$ GeV, where M_Z is the Z boson mass. Events with one or more jets with p_T greater than 25 GeV are rejected. To further reduce the SM backgrounds, we define a kinematic variable ξ constructed using the dilepton p_T and \cancel{E}_T as $|p_T^{\ell\ell} - \cancel{E}_T|/p_T^{\ell\ell}$ where $\ell = e, \mu$.

Signal Regions	Selection Cuts
SRA1	$\cancel{p}_T > 125$ GeV & $\xi < 0.3$
SRB1	$\cancel{p}_T > 150$ GeV & $\xi < 0.5$

Table 8: Signal regions SRA1 and SRB1 defined using the missing energy (\cancel{E}_T) and transverse momentum of the dilepton system where we define $\xi = \frac{|p_T^{\ell\ell} - \cancel{p}_T|}{p_T^{\ell\ell}}$.

The dominant SM background, an irreducible background too, is $pp \rightarrow ZZ \rightarrow \ell^+ \ell^- \nu \bar{\nu} (\ell = e, \mu)$. However, processes like $pp \rightarrow W^+ W^- \rightarrow \ell^+ \nu \ell^- \bar{\nu}$, $WZ \rightarrow \ell \nu \ell^+ \ell^-$ and $ZZ \rightarrow \ell^+ \ell^- \ell^+ \ell^-$ also contribute to the SM backgrounds when additional leptons get misidentified or remain unreconstructed. Two signal regions, SRA1 and SRB1, are constructed using specific choices of cuts on \cancel{E}_T and ξ , see Table 8. The signal region SRB1 is motivated from the ATLAS analysis [81] where \cancel{E}_T is large. The signal region SRA1 is based on our re-optimization of the signal significances with relatively smaller values of \cancel{E}_T and ξ . The number of signal and background events corresponding to each signal regions are shown in Table 9. For both SRA1 and SRB1, we find that one can obtain 5σ statistical significance at the 14 TeV LHC with 3000 fb^{-1} of luminosity, here statistical significance has been calculated as S/\sqrt{B} where S(B) is the number of signal (background) events.

Here we would like to mention that in order to perform this search, the lower limits on the \cancel{E}_T selection cuts need to be restricted to relatively lower values (< 200 GeV) as the signal yield becomes statistically insignificant in the higher \cancel{E}_T regime. The results of this analysis indicate towards a possibility to marginally discover/exclude the heavy Higgses at high luminosity LHC run. However, we would like to mention here that the signal significances have been calculated assuming zero systematic uncertainty. As the systematic uncertainty comes into play, the signal significance will get significantly reduced and will go down much below the 5σ discovery limit.

Signal Regions	Signal		Backgrounds		Significance	
	BP-1	BP-2	ZZ	WZ	BP-1	BP-2
SRA1	921	804	15077	5738	7.45	6.50
SRB1	506	619	9187	3152	5.24	6.41

Table 9: Number of signal and background events at the 14 TeV run of LHC with 3000 fb^{-1} of luminosity obtained after the imposition of our selection cuts for the mono- $Z + \cancel{p}_T$ channel. Here we focus on the first two representative benchmark points BP-1 and BP-2.

3.2.2 Mono-W (leptonic) + \cancel{E}_T channel

Here we present a search strategy for MSSM heavy Higgs bosons in events with a leptonically decaying W boson ($W \rightarrow \ell\nu, \ell = e, \mu$) and significant missing transverse energy for $\sqrt{s} = 14 \text{ TeV}$ run of LHC with an integrated luminosity of 3000 fb^{-1} . The W boson is produced through cascade decay of heavy Higgses, which first decays to a pair of neutralinos and/or charginos, which undergo further decay generating final states containing a W boson and large missing transverse energy. These events generally contain relatively soft leptons or jets. Here we follow the collider strategy as reported in Ref. [82], however some changes have been implemented in order to optimize the signal significances. The representative benchmark point BP-3 has been used to perform the detailed analysis. The decay chains of BP-3 relevant for this analysis are given below:

$$\begin{aligned}
pp &\rightarrow H/A \rightarrow \tilde{\chi}_1^\pm \tilde{\chi}_2^\mp, \quad \tilde{\chi}_2^\mp \rightarrow W^\mp \tilde{\chi}_1^0 \\
pp &\rightarrow H/A \rightarrow \tilde{\chi}_1^0 \tilde{\chi}_{2,3}^0, \quad \tilde{\chi}_{2,3}^0 \rightarrow W^\pm \tilde{\chi}_1^\mp.
\end{aligned}$$

From Table 4, it can be seen that for BP-3, $\tilde{\chi}_1^0$ and $\tilde{\chi}_1^\pm$ are almost degenerate in mass, as a result, $\tilde{\chi}_1^\pm$ undergoes three-body decays resulting into soft leptons or jets in the final state. Similarly, the cascade decay chain originating from H^\pm can also lead to a mono- $W + \cancel{E}_T$ signature. However, we have not considered these decay chains in our analysis because of the relatively smaller production cross-sections of H^\pm .

The candidate events are required to have exactly one isolated electron or muon in the final state with $p_T > 30 \text{ GeV}$. The candidate electron(muon) is required to satisfy $|\eta| < 2.47(2.50)$. The isolation criteria for the candidate leptons is exactly same to what we had discussed in the last section. In addition, events are rejected if they contain one or more jets with $p_T > 25 \text{ GeV}$. For final state topologies with one isolated lepton and missing energy, we usually define a kinematic observable called transverse mass M_T defined using the four momenta of the lepton and \cancel{E}_T as,

$$M_T = \sqrt{2 |p_T^\ell| \cancel{E}_T (1 - \cos(\Delta\Phi_{\ell, \cancel{p}_T}))}$$

where, $\Delta\Phi_{\ell, \cancel{p}_T}$ is the azimuthal angle between the candidate lepton and \cancel{p}_T direction. The dominant source of SM background is the $pp \rightarrow \ell\nu j$ production channel which has been generated with a transverse mass cut $M_T^{\ell\nu} > 100 \text{ GeV}$ where $M_T^{\ell\nu}$ is the transverse mass of the lepton neutrino pair. Besides, processes like diboson production, $t\bar{t}$ etc., also contribute significantly to the background list. Among the diboson modes, the dominant contribution comes from $WZ \rightarrow \ell\nu\nu\bar{\nu}$ and $WW \rightarrow \ell\nu\ell\nu$ ($\ell = e, \mu$) channels.

Signal Regions	Selection Cuts
SRA2	$\cancel{E}_T > 50 \text{ GeV} \quad \& \quad M_T > 175 \text{ GeV}$
SRB2	$\cancel{E}_T > 100 \text{ GeV} \quad \& \quad M_T > 125 \text{ GeV}$

Table 10: Signal regions for the mono- $W + \cancel{E}_T$ analysis. The transverse mass (M_T) is defined using the four momenta of the lepton and the missing transverse momentum \cancel{E}_T .

Similar to the earlier analysis, two signal regions, SRA2 and SRB2, with different optimized values of \cancel{E}_T and M_T , are constructed, as displayed in Table 10. For both the signal regions SRA2 and SRB2, we further selects those leptons which satisfy $|\eta^\ell| < 1.5$ with $\ell = e, \mu$. The choice of these signal regions is driven from the optimization of the signal significances. We investigate several combinations of selection variables \cancel{E}_T and M_T , and among them, two signal regions (SRA2 and SRB2) are chosen which yield the most efficient optimization of signal significances. The expected number of signal and background events at the 14 TeV run of LHC with 3000 fb^{-1} of luminosity are shown in Table 11 for both the above-mentioned signal regions. Similar to our previous analysis, one needs to restrict the lower bounds on \cancel{E}_T to 150 GeV as the signal yields become relatively insignificant as one shifts towards high \cancel{E}_T regime. Here again, we calculate the statistical significance using the signal and background events, and find that it is around 2σ with 3000 fb^{-1} luminosity at the 14 TeV run of LHC. This indicates that it would be very difficult to discover/exclude the heavy Higgs through this channel. More efficient signal optimizations and more precise understanding of the backgrounds may be required to make this search channel more efficient.

Signal Regions	Signal BP-3	Backgrounds					Significance BP-3
		$l\nu$	WW	WZ	$t\bar{t}$	ZZ	
SRA2	6572	$1.0 \cdot 10^7$	76427	68426	58204	9088	2.05
SRB2	5499	$6.8 \cdot 10^6$	47603	52266	59380	8071	2.07

Table 11: Number of signal and background events at the 14 TeV run of LHC with 3000 fb^{-1} of luminosity obtained after the imposition of our selection cuts for the mono- $W + \cancel{E}_T$ channel. Here we focus on the third representative benchmark point BP-3.

3.3 Trilepton + \cancel{E}_T channel

In this section, we present a search strategy for the heavy Higgses H, A, H^\pm in events with leptonically decaying W and Z bosons ($W \rightarrow l\nu, Z \rightarrow \ell\ell, \ell = e, \mu$) produced through cascade decay of heavy Higgses with significant missing transverse energy at $\sqrt{s} = 14 \text{ TeV}$ run of LHC with an integrated luminosity of 3000 fb^{-1} . Here we follow the collider strategy reported in Ref. [83], and consider the representative benchmark point BP-4. The relevant decay chains which generate the above mentioned signature are given below:

$$\begin{aligned}
pp \rightarrow H/A, \quad H/A \rightarrow \tilde{\chi}_1^\pm \tilde{\chi}_2^\mp, \quad \tilde{\chi}_2^\mp \rightarrow W^\mp \tilde{\chi}_3^0, \quad \tilde{\chi}_3^0 \rightarrow Z \tilde{\chi}_1^0 \\
pp \rightarrow H/A, \quad H/A \rightarrow \tilde{\chi}_3^0 \tilde{\chi}_4^0, \quad \tilde{\chi}_3^0 \rightarrow Z \tilde{\chi}_1^0, \quad \tilde{\chi}_4^0 \rightarrow W^\pm \tilde{\chi}_1^\mp,
\end{aligned}$$

In BP-4, $\tilde{\chi}_1^\pm$ undergoes only three body decay resulting in additional leptons or jets in the final state. The cascade decay chain originating from a charged Higgs, with subsequently decays to a chargino-neutralino pair, followed by the decay of charginos and neutralinos to W boson + \cancel{E}_T and Z boson + \cancel{E}_T , respectively, gains a significant branching fraction and leads to a trilepton plus \cancel{E}_T signature. However, because of low production cross-section of H^\pm , the resultant contribution of these decay modes to the trilepton signatures is relatively low. As a result, similar to previous analyses, we have not taken into account the charge Higgs cascade decay chains into our analysis.

The event selection criteria are almost similar to our previous analyses. Candidate events are required to have exactly three isolated leptons (electron/muon) with $p_T > 20$ GeV. The electrons (muons) are required to lie within $|\eta| < 2.47(2.5)$. Isolation criteria discussed in the previous section applies here as well. Among the three candidate leptons, there must be at least one SFOS pair with invariant mass in the range $|M_Z \pm 15|$ GeV. If there are more than one SFOS pairs satisfying the previous condition, then the lepton pair with invariant mass closest to the Z boson mass is finally identified as the SFOS pair. The transverse mass M_T is defined with respect to the lepton which is not a part of the SFOS pair.

Signal Regions	Selection Cuts
SRA2	$\cancel{E}_T > 50$ GeV & $M_T > 150$ GeV
SRB2	$\cancel{E}_T > 50$ GeV & $M_T > 200$ GeV

Table 12: Signal regions for the $3l + \cancel{E}_T$ analysis. The transverse mass (M_T) is defined using the four momenta of the lepton not forming the SFOS pair and the missing transverse momentum \cancel{E}_T .

The SM backgrounds for this search channel are $WZ \rightarrow \ell\nu\ell\ell$ and $ZZ \rightarrow 4\ell$ processes. Here also, we define two signal regions, SRA3 and SRB3, for different conditions of \cancel{E}_T and M_T , as displayed in Table 12. The choice of signal regions are motivated from optimization of signal efficiencies as well as the experimental analysis. The number of signal and background events expected at the 14 TeV run of LHC with 3000 fb^{-1} of luminosity are listed in Table 13. The estimated statistical significances are very small in this search channel, which indicates that probing the MSSM heavy Higgses through trilepton + \cancel{E}_T channel, with leptons originating from the cascade decays of the heavy Higgses, would be an extremely challenging task even at 14 TeV run of LHC.

Signal Regions	Signal	Backgrounds		Significance
	BP-4	WZ	ZZ	BP-4
SRA3	6.92	544	21	0.29
SRB3	4.33	389	16	0.22

Table 13: Number of signal and background events at the 14 TeV run of LHC with 3000 fb^{-1} of luminosity obtained after the imposition of our selection cuts for the $3l + \cancel{E}_T$ channel. Here we focus on the fourth representative benchmark point BP-4.

4 Summary

Precise measurements of the properties of the discovered Higgs boson has been one of the major goals of the LHC physics program. So far, LHC 7 and 8 TeV data reveals that the properties of this new particle are consistent with the SM Higgs boson within the uncertainty in Higgs couplings measurements. Many new physics models beyond the SM contain additional Higgs doublets leading to additional Higgses. A multitude of searches have been performed by the ATLAS and CMS collaborations to probe the heavy Higgses (H, A and H^\pm) of the MSSM through their decay to the SM particles. Note that so far none of these searches have provided a clear signature of the heavier Higgs states. In this regard, it becomes important to examine the non-SM decay modes of the heavier Higgses. The primary motivation for performing such analyses is that when these heavy Higgses decay to light SUSY particles, all the branching ratios to SM particles acquire significant modifications, thereby changes the whole framework of the LHC search strategy. Moreover, there exists certain regions of the parameter space with intermediate $\tan\beta$ (~ 5 -15), where the heavy Higgs couplings to the SM particles become small. However, in this region of interest, one can obtain appreciable amount of non-SM decays which can be studied at the LHC. One such non-SM decay mode could be the decay of the heavy Higgses to the light electroweakinos (charginos and neutralinos). Study of these non-SM decay modes in the light of updated LHC data is precisely the goal of this paper.

In the presence of light SUSY particles, and if kinematically allowed, these heavy Higgs bosons can decay to SUSY particles with a significantly high branching fraction. In order to estimate these non-SM decays, we start with a simple-minded scan making the sparticle sector sufficiently heavy except the electroweakinos, which we assume sufficiently light such that Higgs decay is kinematically allowed, and vary the $\tan\beta$ over a wide range. From this simple analysis, we find that these non-SM ‘ino’ decays can be as large as 70-80% for relatively low values (~ 5 -10) of $\tan\beta$. However, here we do not impose the updated LHC Higgs data and also other low energy flavour data. So, in order to perform a detailed analysis, we scan the MSSM parameter space with the parameters relevant to the electroweakinos, namely M_1, M_2, μ and $\tan\beta$, keeping the sleptons and squarks fixed at high scale. All the scanned points are required to have the lightest Higgs boson mass in the range 122 GeV to 128 GeV. We also consider the constraints from the Higgs couplings measurements, where we use the 95% C.L. contours obtained from a global fit analysis performed by the ATLAS and CMS collaborations. In addition, updated bounds from low energy flavour data in terms on rare b-decays $\text{BR}(b \rightarrow s\gamma)$ and $\text{BR}(B_s \rightarrow \mu^+\mu^-)$ are also considered in our analysis. Now, depending on the values and hierarchy of the electroweakino parameters, we construct ten representative models Model-B to Model-BWH, and then estimate various non-SM ‘ino’ decay modes of the heavy Higgs bosons. From the scan, we observe that some of these ino-modes can be as large as 35-40% even after satisfying the updated LHC data. These non-SM decay modes crucially depends on the gaugino-higgsino mixing, or precisely on the composition of these electroweakino states. However, as we have already mentioned, both the ATLAS and CMS collaborations have searched for additional Higgses at the LHC and put bounds on masses and couplings of these heavy Higgses. So our next task should be to check whether these heavy Higgses, whose non-SM decay modes we are calculating, are still allowed by the current data. Moreover, we also require to perform consistency checks of these light electroweakinos with the

LHC direct search bounds on their masses and couplings obtained at the end of run-I. Instead on implementing the current bounds from the direct searches of the heavy Higgses and electroweakinos on the each points corresponding to our scanned data set, we choose four representative benchmark points making sure that all these points satisfy the current LHC run-I and run-II data.

Once we select those benchmark points consistent with the present LHC data, we ask this simple question, can we utilize this large branching ratios of the heavy Higgses to electroweakinos and look for collider signatures of the same through cascade decay at the 14 TeV high luminosity run of the LHC ? So, we perform dedicated collider analysis at the $\sqrt{s} = 14$ TeV corresponding to an integrated luminosity of 3000 fb^{-1} . We focus on the leptonic modes of the cascade decays as these channels are very clean at the LHC busy environment and also we have better control over the backgrounds. Our collider analysis can be divided into two parts, one focusing on the mono-X plus missing energy signatures where X represents W or Z bosons, and another using the trileptonic channel with significant amount of missing energy. Among the four representative benchmark points, BP-1 and BP-2 are focused to probe the H, A through the mono-Z + \cancel{E}_T signature, while BP-3 and BP-4 are used to study the heavy Higgses through the mono-W + \cancel{E}_T and trilepton + \cancel{E}_T signatures respectively. Following an ATLAS study and making suitable changes in the selection cuts we find that the mono-Z channel has the best sensitivity to probe these heavy Higgses while other two modes posses mild sensitivity for the exclusion of these additional Higgses at the 14 TeV run of LHC with 3000 fb^{-1} luminosity.

Before we end, we would like to note few important issues. In this work, we focus on the decay of the heavy MSSM Higgses to the light electroweakinos only setting other SUSY particles decoupled from the spectrum. However, in principle, some of these sparticles, say top squarks, tau sleptons etc., can be also light, thereby those decay modes will also contribute to the non-SM decay of the heavy Higgses. Moreover, in our collider analysis we restrict ourselves within the leptonic modes only, however plethora of final states involving leptons and jets are possible. Furthermore, some of the final state particles, say W, Z bosons or Higgs bosons, can acquire large transverse momentums, in those situation one need to invoke the state-of-the-art jet substructure techniques to improve the sensitivity of these heavy resonance searches. All of these points are beyond the scope of the current paper, we leave these issues for a future correspondence focussing on the high luminosity runs of the LHC.

Acknowledgements:

Work of B. Bhattacharjee is supported by Department of Science and Technology, Government of INDIA under the Grant Agreement numbers IFA13-PH-75 (INSPIRE Faculty Award). The work of A. Choudhury is supported by the Lancaster-Manchester-Sheffield Consortium for Fundamental Physics under STFC Grant No. ST/L000520/1.

References

- [1] G. Aad *et al.* [ATLAS Collaboration], Phys. Lett. B **716**, 1 (2012) [[arXiv:1207.7214](#)].
- [2] S. Chatrchyan *et al.* [CMS Collaboration], Phys. Lett. B **716**, 30 (2012) [[arXiv:1207.7235](#)].

- [3] The ATLAS and CMS Collaborations, ATLAS-CONF-2015-044 [<http://cds.cern.ch/record/2052552>].
- [4] G. Aad *et al.* [ATLAS Collaboration], *Eur. Phys. J. C* **76**, no. 1, 6 (2016) [[arXiv:1507.04548](https://arxiv.org/abs/1507.04548)].
- [5] V. Khachatryan *et al.* [CMS Collaboration], *Eur. Phys. J. C* **75**, no. 5, 212 (2015) [[arXiv:1412.8662](https://arxiv.org/abs/1412.8662)].
- [6] For reviews on Supersymmetry, see, J. Wess and J. Bagger, *Supersymmetry and Supergravity*, 2nd ed. (Princeton University Press, Princeton, 1991); M. Drees, P. Roy and R. M. Godbole, *Theory and Phenomenology of Sparticles*, (World Scientific, Singapore, 2005); H. E. Haber and G. Kane, *Phys. Rep.* **117**, 75 (1985); H. P. Nilles, *Phys. Rep.* **110**, 1 (1984).
- [7] S. P. Martin, [[arXiv:hep-ph/9709356](https://arxiv.org/abs/hep-ph/9709356)].
- [8] A. Djouadi, *Phys. Rept.* **459**, 1 (2008) [[arXiv:hep-ph/0503173](https://arxiv.org/abs/hep-ph/0503173)].
- [9] [CMS Public SUSY summary](#)
- [10] [ATLAS Public SUSY summary](#)
- [11] G. Aad *et al.* [ATLAS Collaboration], *Phys. Rev. Lett.* **113**, no. 17, 171801 (2014) [[arXiv:1407.6583](https://arxiv.org/abs/1407.6583)].
- [12] V. Khachatryan *et al.* [CMS Collaboration], *Phys. Lett. B* **750**, 494 (2015) [[arXiv:1506.02301](https://arxiv.org/abs/1506.02301)].
- [13] G. Aad *et al.* [ATLAS Collaboration], *JHEP* **1601**, 032 (2016) [[arXiv:1509.00389](https://arxiv.org/abs/1509.00389)].
- [14] V. Khachatryan *et al.* [CMS Collaboration], *JHEP* **1510**, 144 (2015) [[arXiv:1504.00936](https://arxiv.org/abs/1504.00936)].
- [15] G. Aad *et al.* [ATLAS Collaboration], *Eur. Phys. J. C* **76**, no. 1, 45 (2016) [[arXiv:1507.05930](https://arxiv.org/abs/1507.05930)].
- [16] G. Aad *et al.* [ATLAS Collaboration], *Eur. Phys. J. C* **75**, no. 9, 412 (2015) [[arXiv:1506.00285](https://arxiv.org/abs/1506.00285)].
- [17] V. Khachatryan *et al.* [CMS Collaboration], *Phys. Lett. B* **749**, 560 (2015) [[arXiv:1503.04114](https://arxiv.org/abs/1503.04114)].
- [18] G. Aad *et al.* [ATLAS Collaboration], *Phys. Rev. Lett.* **114**, no. 8, 081802 (2015) [[arXiv:1406.5053](https://arxiv.org/abs/1406.5053)].
- [19] V. Khachatryan *et al.* [CMS Collaboration], [[arXiv:1603.06896](https://arxiv.org/abs/1603.06896)].
- [20] G. Aad *et al.* [ATLAS Collaboration], *Phys. Rev. D* **92**, 092004 (2015) [[arXiv:1509.04670](https://arxiv.org/abs/1509.04670)].
- [21] G. Aad *et al.* [ATLAS Collaboration], *Phys. Lett. B* **744**, 163 (2015) [[arXiv:1502.04478](https://arxiv.org/abs/1502.04478)].
- [22] V. Khachatryan *et al.* [CMS Collaboration], *Phys. Lett. B* **748**, 221 (2015) [[arXiv:1504.04710](https://arxiv.org/abs/1504.04710)].
- [23] V. Khachatryan *et al.* [CMS Collaboration], *JHEP* **1410**, 160 (2014) [[arXiv:1408.3316](https://arxiv.org/abs/1408.3316)].
- [24] G. Aad *et al.* [ATLAS Collaboration], *JHEP* **1411**, 056 (2014) [[arXiv:1409.6064](https://arxiv.org/abs/1409.6064)].
- [25] V. Khachatryan *et al.* [CMS Collaboration], *JHEP* **1512**, 178 (2015) [[arXiv:1510.04252](https://arxiv.org/abs/1510.04252)].
- [26] V. Khachatryan *et al.* [CMS Collaboration], *JHEP* **1511**, 018 (2015) [[arXiv:1508.07774](https://arxiv.org/abs/1508.07774)].
- [27] G. Aad *et al.* [ATLAS Collaboration], *JHEP* **1503**, 088 (2015) [[arXiv:1412.6663](https://arxiv.org/abs/1412.6663)].
- [28] G. Aad *et al.* [ATLAS Collaboration], *JHEP* **1603**, 127 (2016) [[arXiv:1512.03704](https://arxiv.org/abs/1512.03704)].
- [29] M. Bisset, J. Li and N. Kersting, [[arXiv:0709.1031](https://arxiv.org/abs/0709.1031)].
- [30] M. Bisset, J. Li, N. Kersting, R. Lu, F. Moortgat and S. Moretti, *JHEP* **0908**, 037 (2009) [[arXiv:0709.1029](https://arxiv.org/abs/0709.1029)].
- [31] A. Arhrib, R. Benbrik, M. Chabab and C. H. Chen, *Phys. Rev. D* **84**, 115012 (2011) [[arXiv:1109.0518](https://arxiv.org/abs/1109.0518)].
- [32] J. F. Gunion, H. E. Haber, M. Drees, D. Karatas, X. Tata, R. Godbole and N. Tracas, *Int. J. Mod. Phys. A* **2**, 1035 (1987).

- [33] J. F. Gunion and H. E. Haber, Nucl. Phys. B **307**, 445 (1988) Erratum: [Nucl. Phys. B **402**, 569 (1993)].
- [34] A. Djouadi, P. Janot, J. Kalinowski and P. M. Zerwas, Phys. Lett. B **376**, 220 (1996) [[arXiv:hep-ph/9603368](#)].
- [35] G. Belanger, F. Boudjema, F. Donato, R. Godbole and S. Rosier-Lees, Nucl. Phys. B **581**, 3 (2000) [[arXiv:hep-ph/0002039](#)].
- [36] M. Bisset, M. Guchait and S. Moretti, Eur. Phys. J. C **19**, 143 (2001) [[arXiv:hep-ph/0010253](#)].
- [37] S. Y. Choi, M. Drees, J. S. Lee and J. Song, Eur. Phys. J. C **25**, 307 (2002) [[arXiv:hep-ph/0204200](#)].
- [38] C. Charlot, R. Salerno and Y. Sirois, J. Phys. G **34**, N1 (2007).
- [39] T. Li, Phys. Lett. B **728**, 77 (2014) [[arXiv:1309.6713](#)].
- [40] G. Belanger, D. Ghosh, R. Godbole and S. Kulkarni, JHEP **1509**, 214 (2015) [[arXiv:1506.00665](#)].
- [41] B. Ananthanarayan, J. Lahiri and P. N. Pandita, Phys. Rev. D **91**, 115025 (2015) [[arXiv:1507.01747](#)].
- [42] A. Djouadi, L. Maiani, A. Polosa, J. Quevillon and V. Riquer, [[arXiv:1502.05653](#)].
- [43] R. Y. Zhang, W. G. Ma, L. H. Wan and Y. Jiang, Phys. Rev. D **65**, 075018 (2002) [[arXiv:hep-ph/0201132](#)].
- [44] T. Ibrahim, Phys. Rev. D **77**, 065028 (2008) [[arXiv:0803.4134](#)].
- [45] S. Heinemeyer and C. Schappacher, Eur. Phys. J. C **75**, no. 5, 230 (2015) [[arXiv:1503.02996](#)].
- [46] ATLAS Collaboration, ATL-PHYS-PUB-2009-079, ATL-COM-PHYS-2009-086.
- [47] F. Moortgat, S. Abdullin and D. Denegri, [[arXiv:hep-ph/0112046](#)].
- [48] A. Djouadi, J. L. Kneur and G. Moultaka, Comput. Phys. Commun. **176**, 426 (2007) [[arXiv:hep-ph/0211331](#)].
- [49] A. Djouadi, J. Kalinowski and M. Spira, Comput. Phys. Commun. **108**, 56 (1998) [[arXiv:hep-ph/9704448](#)].
- [50] Y. Amhis *et al.* [Heavy Flavor Averaging Group (HFAG) Collaboration], [[arXiv:1412.7515](#)].
- [51] G. Degrossi, S. Heinemeyer, W. Hollik, P. Slavich and G. Weiglein, Eur. Phys. J. C **28**, 133 (2003) [[arxiv:hep-ph/0212020](#)]; B. C. Allanach, A. Djouadi, J. L. Kneur, W. Porod and P. Slavich, JHEP **09**, 044 (2004) [[arxiv:hep-ph/0406166](#)]; S. P. Martin, Phys. Rev. D **75**, 055005 (2007) [[arxiv:hep-ph/0701051](#)]; R. V. Harlander, P. Kant, L. Mihaila and M. Steinhauser, Phys. Rev. Lett **100** 191602 (2008) [[arXiv:0803.0672](#)], Erratum: Phys. Rev. Lett **101** 039901 (2008); S. Heinemeyer, O. Stal and G. Weiglein, Phys. Lett. B **710**, 201 (2012) [[arXiv:1112.3026](#)]; A. Arbey, M. Battaglia, A. Djouadi and F. Mahmoudi, [[arXiv:1207.1348](#)].
- [52] A. Djouadi, M. M. Muhlleitner and M. Spira, Acta Phys. Polon. B **38**, 635 (2007) [[arXiv:hep-ph/0609292](#)].
- [53] G. Belanger, F. Boudjema, A. Pukhov and A. Semenov, Comput. Phys. Commun. **185**, 960 (2014) [[arXiv:1305.0237](#)].
- [54] [LEP Higgs Working Group for Higgs boson searches and ALEPH and DELPHI and L3 and OPAL Collaborations], [[arXiv:hep-ex/0107031](#)].
- [55] M. Aaboud *et al.* [ATLAS Collaboration], [[arXiv:1606.03833](#)].

- [56] V. Khachatryan *et al.* [CMS Collaboration], [[arXiv:1606.04093](https://arxiv.org/abs/1606.04093)].
- [57] J. F. Gunion and H. E. Haber, Phys. Rev. D **67**, 075019 (2003) [[arXiv:hep-ph/0207010](https://arxiv.org/abs/hep-ph/0207010)].
- [58] B. Bhattacharjee, A. Chakraborty and A. Choudhury, Phys. Rev. D **92**, no. 9, 093007 (2015) [[arXiv:1504.04308](https://arxiv.org/abs/1504.04308)].
- [59] ATLAS collaboration, ATLAS-CONF-2016-021. [<http://cds.cern.ch/record/2147445>].
- [60] ATLAS collaboration, ATLAS-CONF-2016-016 [<http://cds.cern.ch/record/2141005>].
- [61] B. Bhattacharjee and A. Choudhury, Phys. Rev. D **91**, 073015 (2015) [[arXiv:1407.6866](https://arxiv.org/abs/1407.6866)].
- [62] CMS Collaboration, CMS-PAS-HIG-16-006 [<http://cds.cern.ch/record/2160252>].
- [63] ATLAS collaboration, ATLAS-CONF-2015-061 [<http://cds.cern.ch/record/2114827>].
- [64] ATLAS collaboration, ATLAS-CONF-2016-015 [<http://cds.cern.ch/record/2141003>].
- [65] M. Aaboud *et al.* [ATLAS Collaboration], Phys. Lett. B **759**, 555 (2016) [[arXiv:1603.09203](https://arxiv.org/abs/1603.09203)].
- [66] G. Aad *et al.* [ATLAS Collaboration], JHEP **1404**, 169 (2014) [[arXiv:1402.7029](https://arxiv.org/abs/1402.7029)].
- [67] G. Aad *et al.* [ATLAS Collaboration], JHEP **1405**, 071 (2014) [[arXiv:1403.5294](https://arxiv.org/abs/1403.5294)].
- [68] G. Aad *et al.* [ATLAS Collaboration], JHEP **1410**, 96 (2014) [[arXiv:1407.0350](https://arxiv.org/abs/1407.0350)].
- [69] G. Aad *et al.* [ATLAS Collaboration], Eur. Phys. J. C **75**, 208 (2015) [[arXiv:1501.07110](https://arxiv.org/abs/1501.07110)].
- [70] G. Aad *et al.* [ATLAS Collaboration], [[arXiv:1509.07152](https://arxiv.org/abs/1509.07152)].
- [71] V. Khachatryan *et al.* [CMS Collaboration], Phys. Rev. D **90**, no. 9, 092007 (2014) [[arXiv:1409.3168](https://arxiv.org/abs/1409.3168)].
- [72] V. Khachatryan *et al.* [CMS Collaboration], Eur. Phys. J. C **74**, 3036 (2014) [[arXiv:1405.7570](https://arxiv.org/abs/1405.7570)].
- [73] M. Chakraborti, U. Chattopadhyay, A. Choudhury, A. Datta and S. Poddar, JHEP **1511**, 050 (2015) [[arXiv:1507.01395](https://arxiv.org/abs/1507.01395)].
- [74] A. Choudhury and S. Mondal, [[arXiv:1603.05502](https://arxiv.org/abs/1603.05502)].
- [75] W. Beenakker, R. Hopker and M. Spira, [[arXiv:hep-ph/9611232](https://arxiv.org/abs/hep-ph/9611232)].
- [76] http://www.iacs.res.in/conferences/lhcdm2015/SwB_IACS_Feb2014.pdf
- [77] J. Alwall *et al.*, JHEP **1407**, 079 (2014) [[arXiv:1405.0301](https://arxiv.org/abs/1405.0301)].
- [78] T. Sjostrand, S. Mrenna and P. Z. Skands, JHEP **0605**, 026 (2006) [[arXiv:hep-ph/0603175](https://arxiv.org/abs/hep-ph/0603175)].
- [79] R. V. Harlander, S. Liebler and H. Mantler, Comput. Phys. Commun. **184**, 1605 (2013) [[arXiv:1212.3249](https://arxiv.org/abs/1212.3249)]; R. V. Harlander and W. B. Kilgore, Phys. Rev. Lett. **88**, 201801 (2002) [[arXiv:hep-ph/0201206](https://arxiv.org/abs/hep-ph/0201206)]; Phys. Rev. D **68**, 013001 (2003) [[arXiv:hep-ph/0304035](https://arxiv.org/abs/hep-ph/0304035)]; U. Aglietti, R. Bonciani, G. Degrossi and A. Vicini, Phys. Lett. B **595**, 432 (2004) [[arXiv:hep-ph/0404071](https://arxiv.org/abs/hep-ph/0404071)]; G. Degrossi and P. Slavich, JHEP **1011**, 044 (2010) [[arXiv:1007.3465](https://arxiv.org/abs/1007.3465)]; G. Degrossi, S. Di Vita and P. Slavich, JHEP **1108**, 128 (2011) [[arXiv:1107.0914](https://arxiv.org/abs/1107.0914)]; R. Harlander and P. Kant, JHEP **0512**, 015 (2005) [[arXiv:hep-ph/0509189](https://arxiv.org/abs/hep-ph/0509189)].
- [80] J. de Favereau *et al.* [DELPHES 3 Collaboration], JHEP **1402**, 057 (2014) [[arXiv:1307.6346](https://arxiv.org/abs/1307.6346)].
- [81] G. Aad *et al.* [ATLAS Collaboration], Phys. Rev. D **90**, no. 1, 012004 (2014) [[arXiv:1404.0051](https://arxiv.org/abs/1404.0051)].
- [82] ATLAS collaboration, ATLAS-CONF-2014-017 [<https://cds.cern.ch/record/1692660>].
- [83] ATLAS Collaboration, ATLAS-PHYS-PUB-2014-010 [<https://cds.cern.ch/record/1735031>].